

Th-U-Pb_T Dating by Electron Probe Microanalysis, Part I. Monazite: Analytical Procedures and Data Treatment

Datação Th-U-Pb_T com Microsonda Eletrônica, Parte I. *Monazita: Procedimentos Analíticos e Tratamento de Dados*

Silvio Roberto Farias Vlach (srfvlach@usp.br)
Departamento de Mineralogia e Geotectônica - Instituto de Geociências - USP
R. do Lago 562, CEP 05508-080, São Paulo, SP, BR

Received 09 September 2009; accepted 18 December 2009

ABSTRACT

Dating methodology by the electron probe microanalyser (EPMA) of (Th, U)-bearing minerals, highlighting monazite, acquired greater than ever importance in literature, particularly due to its superior spatial resolution, as well as versatility, which allow correlating petrological processes at times registered only in micro-scales in minerals and rocks with absolute ages. Although the accuracy is inferior to the one achieved with conventional isotopic methods in up to an order of magnitude, EPMA is the instrument that allows the best spatial resolution, reaching a few μm^3 in some conditions. Quantification of minor and trace elements with suitable precision and accuracy involves the own instrumental and analytical set-ups and data treatment strategies, significantly more rigorous when compared with those applied in conventional analyses. Th-U-Pb_T dating is an example of these cases. Each EPMA is a unique machine as for its instrumental characteristics and respective automation system. In such a way, analytical procedures ought to be adjusted for laboratory specificities. The analytical strategies and data treatment adopted in the Electronic Microprobe Laboratory from *Instituto de Geociências of Universidade de São Paulo*, Brazil, with a JEOL JXA8600S EPMA, and a ThermoNoran-Voyager 4.3 automation system, are presented and compared with the ones used in other laboratories. The influence of instrumental factors and spectral overlaps on Th, U, and Pb quantification is discussed. Applied procedures to interference correction, error propagation, data treatment, and final chemical age presentation as well as to sampling and analyses are emphasized. Some typical applications are discussed, drawing attention to the most relevant aspects of electron microprobe dating.

Keywords: Th-U-total Pb dating; Monazite; Microanalysis; Electron probe microanalyser (EPMA).

RESUMO

A metodologia de datação de minerais portadores de Th e/ou U com microsonda eletrônica (EPMA), com ênfase em monazita, adquiriu enorme importância em literatura, devido a sua alta resolução espacial e versatilidade, que permitem correlacionar processos petrológicos, por vezes registrados apenas em microescala em minerais e rocha, com idades absolutas. Embora a acurácia seja até uma ordem de grandeza inferior à alcançada com os métodos isotópicos convencionais, o EPMA é o equipamento que resulta na melhor resolução espacial, alcançando alguns poucos μm^3 sob algumas condições. A quantificação de elementos menores e em traços com precisão e acurácia adequadas envolve estratégias instrumentais, analíticas e de tratamento de dados específicas e significativamente mais rigorosas quando comparadas com as empregadas em análises convencionais. A datação Th-U-Pb_T é um exemplo destes casos. Cada EPMA é um aparelho único em função de suas características instrumentais e sistema de automação e, desta forma, os procedimentos analíticos devem ser ajustados para as especificidades de cada laboratório. As estratégias analíticas e de tratamento de dados adotadas no Laboratório de Microsonda Eletrônica do Instituto de Geociências da Universidade de São Paulo, Brasil, com um equipamento JEOL JXA8600S e sistema de automação ThermoNoran-Voyager 4.3 são apresentadas e comparadas com similares aplicadas em outros laboratórios. A influência de fatores instrumentais e das interferências espectrais para a quantificação de Th, U e Pb é discutida. Os procedimentos para correções de interferências, propagação de erros, tratamento e apresentação dos resultados finais de idades químicas, bem como de amostragem e análise são enfatizados. Alguns exemplos típicos de aplicação são discutidos, ressaltando os aspectos mais relevantes associados à datação com microsonda eletrônica.

Palavras-chave: Datação Th-U-Pb total; Monazita; Microanálise; Microsonda eletrônica (EPMA).

INTRODUCTION

Since the first applications in uraninite and thorite (e.g., Parslow et al., 1985; Bowles, 1990), Th-U-Pb_T dating with electron probe microanalyser (EPMA) experienced great development during the last years. EPMA high spatial resolution, allied to texturally well-controlled chemical and geochronological information simultaneously obtained in thin polished sections, promote its increasing application.

Over the last decades, chemical dating has been applied to distinct (Th, U)-bearing minerals, such as monazite, xenotime, zircon, and uraninite (e.g., Suzuki and Adachi, 1991; Montel et al., 1996; Cocherie et al., 1998; Williams, Jercinovic, Terry, 1999; Geisler and Schleicher, 2000; Kempe, 2003). Monazite [(Ce, La, Nd, Th) PO₄] is one of the most appropriated and used mineral. It does not incorporate significant amounts of Pb when its formation took place (e.g., Parrish, 1990), and contains Th and U abundances that generate measurable radiogenic Pb contents in geologically reduced time interval. Pb diffusion in the structure of monazite is very low under crustal environments (e.g., Cherniak et al., 2004, Gardés et al., 2007), and it presents relatively wide distribution in continental crust. Monazite appears as primary accessory phase in several igneous, average- to high-grade metamorphic, pegmatite, and diverse hydrothermal rocks; as a detritic phase, in psamitic sediments and rocks (e.g., Overstreet, 1967; Chang, Howie, Zussman, 1998). An unusual occurrence is described in lunar basalts by Lovering et al. (1974). The chemical composition of monazite allows also studies concerning LREE saturation conditions in magmatic systems (e.g., Rapp and Watson, 1986; Montel, 1993) and geothermometry of igneous and metamorphic rocks (e.g., Gratz and Heinrich, 1998, Pyle et al., 2001).

These characteristics convert monazite chemistry and chemical dating in powerful tools to settle geological problems with complex evolutionary history involving superposition of discrete tectonic and/or petrologic processes during geologic time, placing them under a new perspective. This potential incentivized the development of analytical-instrumental procedures and refined data treatment, aiming at obtaining precise and accurate chemical compositions as well as ages (e.g., Cocherie et al., 1998; Pyle et al., 2005; Jercinovic and Williams, 2005) that also have brought significant contribution to trace element analysis accomplished with EPMA.

Monazite, xenotime and zircon EPMA dating was first done by Suzuki and Adachi (1991), who developed the CHIME method (CHemical Isochron METHod). Determination of point ages in monazite and its statistical treatment were elaborated by Montel et al. (1996), while Williams, Jercinovic and Terry (1999) obtained the first age

distribution maps in a single crystal. The method is simple and based on Th, U, Pb_T quantification with suitable precision and accuracy. However, factors including since sample preparation, instrumental setup, calibration, and intensity readings, until data treatment introduce several error types whose approach requires specific cares (e.g., Scherrer et al., 2000; Pyle et al., 2005; Jercinovic and Williams, 2005; Lisowiec, 2006; Spear, Pyle, Cherniak, 2009).

Procedures for monazite, xenotime, and thorite dating were developed in our EPMA Laboratory years ago (Vlach, Gualda, Chiessi, 1999a, 1999b), and since then have been optimized and applied to different geological situations (e.g., Vlach and Gualda, 2000; Vlach and Del Lama, 2002; Vlach et al., 2003; Martins, Vlach, Janasi, 2009). In this work, a review of concepts and main factors that affect method precision and accuracy, with emphasis on monazite, as well as the analytical approach applied are presented. Advantages and disadvantages of different models for data reduction and treatment, as well as examples of application to typical geological situations are discussed.

THEORETICAL FOUNDATION AND PREMISES

In a Th and U closed system, after a certain time interval, the total amount of Pb will be equal to the sum of Pb initially present (Pb₀, initial or common) with the one produced by Th and U radioactive isotope decay. After reaching a secular balance in the ²³²Th, ²³⁵U, and ²³⁸U radioactive series, stable Pb isotopic production ratio (²⁰⁸Pb, ²⁰⁷Pb, and ²⁰⁶Pb respectively) is proportional to the radioactive decay of the parent isotopes. The total Pb in the reference system is given by the contribution of these three radioactive series, resulting in the following transcendental equation:

$$Pb_T = Pb_0 + Th \times K^{Th} \times (\exp^{(232\lambda_{Th}t)} - 1) + U \times [K^{U8} \times (\exp^{(238\lambda_U t)} - 1) + K^{U5} \times (\exp^{(235\lambda_U t)} - 1)] \quad (1)$$

where Pb_T, Th and U are total Pb, Th, and U contents (% weight) present after the elapsed time (*t*, yr), Pb₀ is the initial Pb amount (*t* = 0), and λ is the constant of radioactive decay (²³²λ_{Th} = 4.94752E-11, ²³⁸λ_U = 15.5125E-11, and ²³⁵λ_U = 98.4850E-11, given in yr⁻¹, Steiger and Jäger, 1977). K constants contemplate relative isotopic abundances (Ab), and elemental atomic masses (Ar): KTh = (Ab²³²Th)*(Ar²⁰⁸Pb)/(ArTh), K^{U8} = (Ab²³⁸U)*(Ar²⁰⁶Pb)/(ArU), K^{U5} = (Ab²³⁵U)*(Ar²⁰⁷Pb)/(ArU), and their values are 0.896405, 0.859157, and 0.006261, respectively.

Equation (1) is the fundamental equation for age calculation in closed systems, since the actual Th, U and Pb_T measured amounts, when Pb₀ is known, is insignificant in relation to Pb_T, or even constant. There are not full

guaranties that embedded premises are always valid, and dating results should be taken *a priori* as dates to which ages status are attributed when they have geological significance and representativeness.

In general, the amounts of common Pb in monazite may be considered negligible, rarely exceeding ca. 1% of the radiogenic Pb accumulated in a few hundreds of Myr (Parrish, 1990; Kingsbury et al., 1993). Pb is stable in monazite structure (Podor and Cuney, 1997), and presents very low diffusion coefficients in most geological processes occurring in the continental crust (Seydoux-Guillaume et al., 2002; Cherniak et al., 2004; Gardés et al., 2007). The monazite structure is also very resistant to metamictization processes (Karioris, Gowda, Cartz, 1991).

INSTRUMENTAL AND ANALYTICAL CONDITIONS

Analysis of elements with concentrations below 10,000 ppm with EPMA requires a careful examination of instrumental and analytical conditions, becoming interesting challenges at times. It happens with chemical dating, once suitable minerals could present Th and/or U, and particularly Pb_T amounts in this order of magnitude. Additionally, there are several possible instrumental configurations to an EPMA (e.g., Goldstein et al., 1992; Reed, 1993), and even in equivalent equipments, each component presents their own characteristics, and must be considered unique.

Analytical procedure optimization aims at obtaining quantitative data with suitable precision and accuracy to the age-determining elements (Th, U, Pb_T) in a compatible time interval by using as simple approach as possible. The main factors to be considered are discussed following, after a presentation of available instrumental in the laboratory.

Instrumentation

The EPMA from the Instituto de Geociências of the Universidade de São Paulo is a JEOL-JXA8600S equipment with 5 wavelength dispersive (WD) spectrometers with a 140 mm Rowland Circle. Each spectrometer possesses two interchangeable Johann type analyzer crystals, two of them (E1 with STE/TAP, E2 with TAP/PET crystals) are provided with flow proportional counters with polypropylene window; a mixture of ca. 90% Ar + 10% methane (P10) flows under atmospheric pressure. The three other (E3-E5, PET/LiF crystals) present counters sealed with a thin Be window, filled with Xe under low pressure (< 60 torr). X-ray windows with slots of 300, 500, and 3,000 μm allow minimizing scatter effects in relation to ideal Bragg diffraction angle. X-ray take-off angle is 40°, and spectral syntonization positions are the distances (L) from the centre

of analyzer crystal to the incidence point of the electronic beam over sample:

$$L(mm) = n \times \frac{R}{d} \times \lambda \quad (2)$$

where R (mm) is Rowland Circle radius; d (Å) is the interplanar spacing of the analyzer crystal; λ (Å) is the radiation wavelength; n is the diffraction order, and 60 ≤ L ≤ 260. Minimal step of the spectrometer motor is 0.005 mm.

System is coupled to a NORAN energy dispersive spectrometer (EDS), and THERMO-NORAN Voyager automation system (version 4.3). Corrections for matrix effects and data reduction are routinely accomplished with the PROZA systematic (e.g., Bastin and Heijligers, 1990).

A nitrogen cold finger could be used to minimize sample contamination and damage. EPMA and automation system are connected to a clean energy line provided by a no-break group, fed by net or, alternatively, by a generator group, providing great stability besides avoiding interruptions during routine work. The machine is turned-off only for maintenance. The EPMA room is isolated and its temperature is controlled by air-split type refrigerator; temperature variations inside the main chamber and spectrometers are estimated to be lower than 1°C.

Polished rock thin sections are prepared with an automatic, high precision PM4 Logitech equipment of lapping and polishing by using alumina. Grains are mounted over thin glass sections with conventional resin, and then polished. Sections and mounts are C-coated with an Auto-306 Edwards Instruments evaporator under 2.10⁻⁵ torr of vacuum. Coating thickness (250 ± 15 nm) is controlled with a fine quartz film.

A MicroBeam automatic Digimax stage coupled to a petrographic microscope with transmitted and reflected lights is conventionally used to set (x, y) point-coordinates with high precision. A spreadsheet converts them to equivalent EPMA stage values.

Instrumental setup

The choice of incident electronic beam conditions depends on sample composition, and it is always a commitment among many factors, such as spatial resolution, matrix effects, counting statistics, and sample damage. It may be a hard task, particularly when the sample contains both light and heavy elements. The maximization of counts, P/B ratio (ratio between peak and background intensities) and spatial resolution as well as the minimization of detection limits and sample damage are the objectives to be pursued. Acceleration voltage of the electronic column and beam current are the main parameters to be considered but

procedures that involve high signal intensities and problems with spectral interferences require specific cares with dead-time effects and Pulse Height Analyses (PHA) in the Single Channel Analyzer (SCA). Setting collimator window slots to narrow values optimizes P/B ratio, and increases spectral resolution. However, it entails disadvantages related to total intensities reduction and sample focus, among others (e.g., Reed, 1993). In the adopted procedure, slots are placed at maximum width. Electrostatic deflectors prevent X-ray detectors from electron entrance.

Electronic column acceleration voltage

The characteristic X-ray intensity depends on overvoltage (U , the ratio between incident beam energy, E_0 , and critical excitation energy of a determined spectral line, E_c), which could be approached to $(U - 1)^{1.67}$ (e.g., Reed, 1993). In general, values between 2 and 3 are appropriate to achieve suitable signals. Critical excitation energy for measured lines of elements of interest in monazite are between 1.84 keV (Si K) and ca. 7.0 keV (MREE L); Th, U and Pb present 3.32, 3.56, and 2.50 keV M line energies, respectively. Thus, a minimal value of $E_0 \approx 15$ keV is necessary. In the literature, values between 15 and 25 kV to column acceleration voltage were suggested (Williams, 1996; Scherrer et al., 2000). Overvoltage increase results in higher P/B ratio intensities and lower detection limits. However, electron penetration into the sample is high, increasing X-ray production volume and absorption, therefore decreasing spatial and analytical resolution.

Simulations of electron interaction volumes and X-ray production for Ce, Th, U, and Pb were presented by Pyle et al. (2005). For monazite compositions with moderate and high Th contents, the authors show that they are similar at 15 keV, but well contrasted under 25 keV electron beam energy. Nonetheless, the volumes of X-ray emissions are more relevant. Figure 1 presents $\phi(\rho z)$ X-ray generation and emission curves calculated for elements of interest in monazite with typical composition at 15 and 25 keV energies. These diagrams show that spatial resolutions obtained for 15 keV is much superior than the one obtained for 25 keV. They also show that the ratio between emitted and produced X-rays is much inferior for 25 keV, owing to higher sample absorption. Importantly, under 25 keV the emission volumes of characteristic Pb M X-ray lines are significantly shallower than Th M, and U M volumes. Same comparisons could be done between the first ones and Y L lines volumes. The later are shallower, as well as the volumes of Si K and P K (not presented). Analyses will lose quality if there are significant compositional variations at this scale. Additionally, a high voltage should accentuate secondary fluorescence effects close to limits between domains with contrasted compositions.

The use of a 15 kV column acceleration voltage is more suitable, thus, to solve minor scale compositional variations. Higher (20, 25 kV) voltages could be used to homogeneous crystal, gaining some analytical precision (Scherrer et al., 2000; Pyle et al., 2005). However, the gain in average population age errors calculated in dating procedure is small.

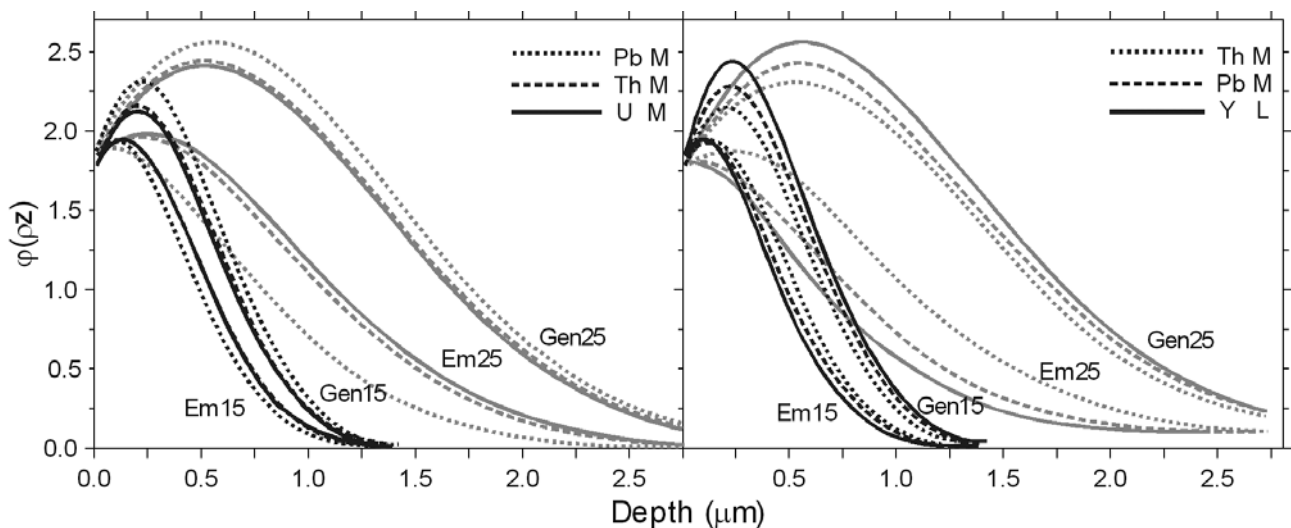


Figure 1. $\phi(\rho z)$ curves illustrating the distribution of generated (Ge) and emitted (Em) X-rays with depth for 15 and 25 keV incident electronic beam energies for analyzed critical-element spectral lines in a typical monazite with Th = 6.0, U = 0.50, La = 14.0, Ce = 27.0, Nd = 10.0, Y = 0.50, Pb = 0.50, P = 13.5, and O = 28.0 (% wt.), $\rho = 5$ g/cm³. Difference between areas under generation and emission curves corresponds to X-ray absorbed by sample.

Electronic beam current and diameter

For a given voltage, signal intensity increases with electronic beam current. However, the higher the current, the higher the minimal diameter of the electronic beam, and the higher the temperature increase in the impact point over the sample, leading to sample damage. Temperature variation at the beam impact point is expressed in the equation from Castaing (1951):

$$\Delta T (^{\circ}K) = 4.8 \times \frac{i_B \times E_0}{\lambda_T \times d} \quad (3)$$

where i_B (μA) is the current; E_0 (keV) is the energy, and d (μm) is the diameter of the electronic beam. λ_T is the sample thermal conductivity constant (W/cmK), which varies between 0 and 1; the higher value is attained in metals. Taking $E_0 = 20$ and $d = 1$, a beam current of 300 nA results in ΔT variations of $290^{\circ}K$ for typical λ_T values (0.1) of crystalline materials, 15 times higher than the ones produced under 20 nA. The increase of beam diameter partially avoids this problem, although it decreases spatial resolution.

Sample damage changes both measured X-ray and absorbed (sample) current intensities. High-quality coating as well as an efficient link between coating-film and sample holder are needed. The relatively low C electrical and thermal conductivities could lead severe sample damage under high currents (e.g., Goldstein et al., 1992). The combination of higher voltage with lower currents could be a solution in some cases. Au coating minimizes this effect but introduces undesirable Au M γ family lines in spectral zones of interest for chemical dating as well as increases X-ray absorption (Jercinovic and Williams, 2005). Also, it makes difficult the use of same standards for dating and conventional analyses. Lighter elements (P, Si, and S when present) migration or even volatilization increases intensity signals of heavier elements (Th, U, Pb, and REE). Jercinovic and Williams (2005) show a significant backscattering coefficient, and so mean atomic number, increase in analyzed points over monazite coated with C. If evaporation takes place, holes could be produced at the beam impact point, and the surface should not remain flat (Reed, 1993).

Laboratory tests under varied current, beam diameter, and counting time settings with crystals with contrasted compositions show that 300 nA, 2 - 4 μm , and 400 s values are acceptable to common monazite compositions, and the introduced errors could be considered within systematic errors. Figure 2 illustrates signal intensity, measured for Ce L α , Th M α , U M β , Y L α , and Pb M α , variations through time. Between 0 and 450 s, Th, U, Y and Pb intensities seem to be constant but Ce, the most abundant element,

presents a slight and progressive increase up to ca. 450 s, going from average values of 3,300 to 3,350 cps (1.5%), followed by an abrupt fall to 3,200 cps; this fall also affects the other elements. After 550 s, a 4% fall was observed in the absorbed current.

In order to minimize these effect, U and Pb are simultaneously read; Th is read together, after P, and S if needed, readings. The Voyager system updates the absorbed current readings each second, allowing the operator to evaluate sample damage in real time. For a 300 nA beam current, the absorbed current varies between ca. 220 and 205 nA depending on monazite composition. Simple tests at the beginning of an analytical routine will evidence, or not, any abrupt changes, as well as the variations of the absorbed current through the required time. The beam current and/or total counting time could be decreased as necessary.

Dead-time and pulse height analyses (PHA)

Measured intensities need to be corrected for dead-time. This effect is particularly relevant when high counting ratios are involved, and when counting ratios are much different in standards and samples. The dead-time is specific to each spectrometer and its value depends on characteristics and setup of the detectors, and the electronics involved in signal amplification and transmission (e.g., Goldstein et al., 1992; Reed, 1993). Typical values are between 1 and 2 μs , so that for a 2 μs value, a measured 10,000 cps correspond to actual 10,200 cps (2%) intensity. Under 15 kV and 300 nA, the standards UO₂, ThSiO₄, PbS, PbCr₂O₄, YAlG (synthetic Y-Al garnet), and YPO₄ standards give liquid counts about 40,500, 17,000, 21,000, 15,000, 102,000, and 117,000 cps to U M β , Th M α , Pb M α e Y L α lines in our lab, while a typical

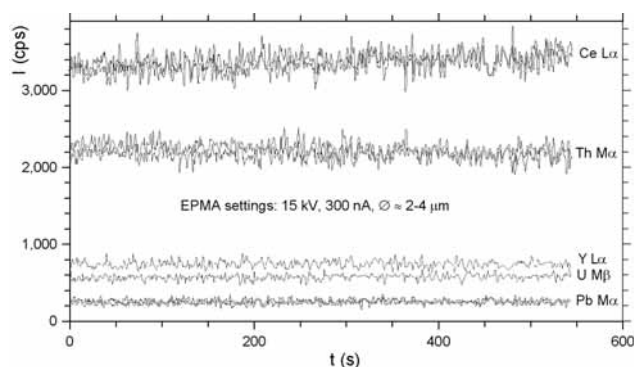


Figure 2. Diagram illustrating variations of Ce, Th, Y, U and Pb spectral line intensities in the E5, E2, E1, E3 and E4 spectrometers, respectively, as a function of the elapsed time for a monazite reference crystal under the electronic beam, for the indicated instrumental conditions (monazite from a biotite monzogranite, sample APAB-956).

monazite ($\text{UO}_2 = 0.19$, $\text{ThO}_2 = 4.4$, $\text{PbO} = 0.18$ and $\text{Y}_2\text{O}_3 = 1.9$ wt%) gives 62, 800, 30, and 2,940 cps, respectively.

Dead-time should be experimentally determined for each spectrometer, and can be obtained by plotting the ratio between measured intensities and beam current *vs.* measured intensities (e.g., Reed, 1993) by using, for instance, standard readings under varied beam currents. In our instrument, values varies from 2.4 (E1) to 1.8 (E2), and between 1.5 and 1.2 (E3, E4, and E5) μs .

Pulse voltage in SCA depends, among other electronic factors, on the photon energy, amplifier gain, and the voltage applied to detectors, as well as the type of detector (acc. Goldstein et al., 1992). Selection of an energy window, establishing a baseline and window interval in SCA (differential mode), allows filtering pulses due to noise, background radiation, spectral interferences, and pulses arising out of diffraction orders above 1, when the ranges of their energies and the energy range of the characteristic pulse to be measured are distinct. A necessary caution, when dealing with high counting rates, is related to drift possibility in pulse distribution toward lower voltages, crossing over the established baseline, and leading to count losses (e.g., Goldstein et al., 1992; Reed, 1993). The use of differential mode is essential in monazite analysis to minimize interferences and optimize P/B ratio, but the PHA setup should take into consideration the standards to be used, once some of them give count rates up to 3 orders of magnitude superior.

Elemental setup: spectral interferences, outlines, and corrections

One of the challenging aspects in monazite analysis is the presence of interferences over the spectral lines of interest of the REEs and age-determining elements. Among them, several could be eliminated when spectral lines and/or off-sets to background readings and/or suitable energy windows are selected, after detailed WD spectrum and PHA distribution analyses. Always when it is possible this procedure should be done. Nevertheless, some interferences could not be avoided, and need correction. Procedures for several REE-bearing mineral analyses were exhaustively discussed in the literature (e.g., Williams, 1996; Reed and Buckley, 1998), so only relevant elements for monazite dating will be emphasized. The protocol used in the laboratory for Ce-monazite analysis and dating is summarized in Table 1.

WD spectral analyses

Spectral resolution depends on geometrical factors of the analyzer crystal, the Rowland Circle radius (Reed, 1993), and equipment characteristics. Mathematical modeling

allows a good approach for WD spectra under selected conditions to evaluating interference problems and defining *a priori* analytical parameters, to be experimentally refined. The Virtual WDS program (Reed and Buckley, 1996) is routinely used to this task.

Th, U, and Pb M lines are quantified using PET crystals. $\text{M}\alpha$ lines give intensities up to ca. 30% higher than $\text{M}\beta$ lines, and are more suitable. With flow detector (P10), however, the intensities of the U $\text{M}\beta$ and $\text{M}\alpha$ are close due to Ar $\text{K}\alpha$ absorption (acc. Goldstein et al., 1992, see below). Anyway, U $\text{M}\beta$ line is preferred because the severe interference of Th $\text{M}\beta$ over U $\text{M}\alpha$.

PET crystals present excellent reflectivity but relatively low resolution; besides, they deteriorate easier than TAP and LIF crystals, and present higher linear expansion coefficient (ca. $1.2\text{E-}4 \perp (002)$, acc. Jenkins and DeVries, 1982) turning them much susceptible to temperature variations, which provoke line position shifts. In a typical spectrometer, $(\Delta L)/^\circ\text{C}$ variations amount to 0.015, 0.018, and 0.025 mm in U $\text{M}\beta$ (119.02), Th $\text{M}\alpha$ (132.54), and Pb $\text{M}\alpha$ (169.31) L positions, respectively. Pyle et al. (2005) estimate an intensity loss of ca. 20% of Pb $\text{M}\alpha$ due to a variation of 5°C . Of course, this effect increases with L, and measured intensities of P $\text{K}\alpha$ ($L = 197.24$ mm, $(\Delta L)/^\circ\text{C} \cong 0.035$) should be used to monitor it, which appear to be not much relevant in our lab.

The type of detector (P10 *vs.* Xe) results in significant differences in the spectral range of interest. The Ar K absorption line (3.202 keV, $L_A = 123.98$ mm) leads to significant decrease of the continuous radiation intensity at higher L_A values, and significantly increases P/B ratios (e.g., Goldstein et al., 1992), while the Xe L absorption line appears only at $L = 72.82$ mm. The energies of Ar $\text{K}\alpha$ (2.957 keV) and Xe $\text{L}\alpha_1$ (4.109 keV) generate their own escape peaks. The escape peak intensity is about 5% of intensity of main peak in the first case, but very inferior in the second, as the difficulty of absorption of the Xe L lines in the gas is much higher (Reed, 1993). The influence of these factors to U and Pb setup is analyzed by Pyle et al. (2005). In our lab, both elements are read in Xe-type spectrometers, while Th is read with (P10)-type spectrometer.

Th $\text{M}\alpha$ line is the easiest to be measured. Minor interferences in the regions of interest for background readings include Nd $\text{L}\beta_{2-15}$, Ce Ly, Gd $\text{L}\alpha_1$ and La Ly lines in negative side (lower offset), and Nd $\text{L}\beta_6$ in positive side (higher offset). They are second-order lines that can be eliminated or minimized, at least, through PHA. Nevertheless, care must be taken when dealing with samples with low Th and high Nd and/or Gd contents; Ar $\text{K}\alpha$ -Gd $\text{L}\alpha_1$ escape peak and Th $\text{M}\alpha$ have similar energies, for instance. The effect of this late interference is minor for the low Gd concentrations found in most common monazite.

Table 1. Instrumental and elemental set-ups for Ce-monazite analysis and dating in the EPMA Lab from *Instituto de Geociências of Universidade de São Paulo*. Bck+, Bck- are positive and negative off-sets to linear interpolation of background intensity under analyzed spectral line. BsL and Win are Baseline and Energy Window values (V). Standards: n = natural mineral; without identification = synthetic composites. * = spectral lines to which there is not a measurable off-set position. § = critical off-sets, depending on analyzed monazite composition. See text.

I. Setup: [Ce-monazite (Z ≈ 41) CHV : 15 kV Beam : 300 nA, Ø ≈ 2 - 3 µm]

##	Elm	Line	Crystal	LPos (mm)	Bck-	Bck+	BsL	Win	Standard
1	Si	Kα	TAP	77.330	1.650 [§]	1.050	1.12	4.00	ThSiO ₄
2	Th	Mα	PET (P10)	132.240	1.800 [§]	1.600	0.72	2.40	ThSiO ₄
3	U	Mβ	PET (Xe)	119.000	3.980 [§]	3.980	1.32	2.40	UO ₂
4	Al	Kα	TAP	90.580	3.250 [§]	0.850	1.04	4.00	YAlG
5	La	Lα	LIF	185.320	1.450	1.650	0.68	2.00	LaPO ₄
6	Ce	Lα	LIF	178.070	1.450	1.650	0.72	2.00	CePO ₄
7	Pr	Lβ	LIF	157.030	0.750	0.850	0.92	2.00	PrPO ₄
8	Nd	Lβ	LIF	150.660	0.900	1.000	0.96	2.00	NdPO ₄
9	Sm	Lβ	LIF	138.950	0.550	0.550	1.12	2.00	SmPO ₄
10	Gd	Lβ	LIF	128.420	1.000	1.000	1.32	2.00	GdPO ₄
11	Tb*	Lβ	LIF	123.590	0.450	-	1.42	2.00	REE1
12	Dy	Lβ	LIF	118.990	0.650	0.550 [§]	1.44	2.00	DyPO ₄
13	Er*	Lα	LIF	124.110	0.750	-	1.36	2.00	REE1
14	Yb*	Lα	LIF	116.250	-	1.450	1.48	2.00	YbPO ₄
15	Y	Lα	TAP	69.980	1.250	0.700	1.24	4.00	YPO ₄ /YAlG
16	Fe	Kα	LiF	134.640	0.750 [§]	0.650	1.16	2.24	Hematite ⁿ
17	Ca	Kα	LIF	233.570	0.700	1.100	0.60	1.52	Ca2P/Titanite ⁿ
18	Pb	Mα	PET(Xe)	169.250	3.650	3.900 [§]	0.48	2.32	PbCr ₂ O ₄ / PbS ^{n§}
24	P	Kα	PET(P10)	196.900	2.100	2.650	0.64	2.00	NdPO ₄
25	S*	Kα	PET(P10)	171.940	-	2.000	0.68	2.00	PbS ⁿ

II. Spectrometer, detector Bias (V), element, and total counting time [T_T (s)] distribution

#Run	TAP1, 1716	PET2, 1690	PET3, 1690	PET4, 1724	LiF5, 1664
1	Y (30)	P (20)	U (400)	Pb (400)	Ca (20)
2	Si (20)	Th (280)			La (20)
3	Al (30)				Ce (20)
4					Pr (20)
5					Nd (20)
6					Sm (40)
7					Fe (20)
8					Gd (40)
9					Dy (40)
10					Yb (40)

$$T_T = T_{\text{peak}} + T_{\text{back}}$$

Relevant interferences for U Mβ and Pb Mα quantification are highlighted by Susuki e Adachi (1991), Scherrer et al. (2000), and Pyle et al. (2005), among others. Detailed WDS scanning of the regions of interest obtained with our equipment are presented in Figures 3 and 4.

The U Mβ line presents severe first-order Th M line interferences, particularly of Th Mγ, as well as K Kα, and Th AM5 abs line (Figure 3). Th interferences can be avoided or numerically corrected (acc. following item), and K is typically absent in common monazite. Minor interferences are produced by Ho Lα and Gd Lβ (n = 2) line family. Several second-order lines, as Lα2 lines and Eu, Gd and Pr Lβ family appear in negative background off-set region, while Th M4-O2 lines, Nd and Pr Lγ, Sm Lβ2-15, Dy Lα2, Eu Lβ and Yb Lγ lines in positive background off-set region. Except for Th and K lines and Xe Lα1-Nd Lγ escape peak, these interferences are eliminated adjusting a suitable window in SCA. We estimate the background intensity through linear interpolation of ± 3.9 off-set readings (Figure 3). Continuous spectral modeling (e.g., Reed and Buckley, 1996) indicates that background values obtained in such a way are overestimated by ca. 0.15%, so measured U abundances are underestimated in ca. 30 ppm.

The Pb Mα line presents interferences of Th Mζ1, 2 and Y Lγ 2, 3 lines; the first lines affect both characteristic position and background regions of interest, while the other ones affect the characteristic. Ce (Lα1, Lα2 LN) and ThM2-O4 second-order lines as well as Y AL1 interfere on the negative background off-

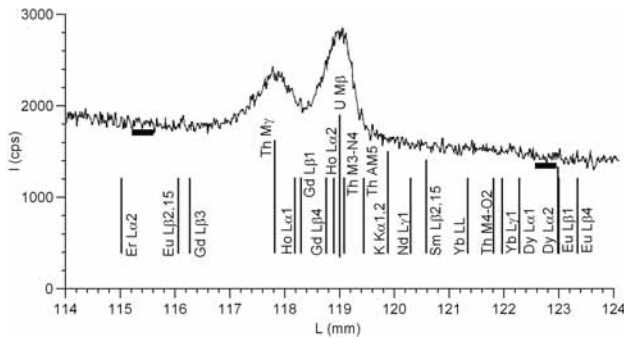


Figure 3. WDS step scanning for the region of interest to U Mβ for a monazite crystal from the Varginha garnet-kyanite granulite (VGr reference sample). Measured intensities (I_i) were smoothed by the function:

$$I_i = \frac{I_{i-2} + I_{i+2}}{4} + \frac{I_{i-1} + I_{i+1}}{2}$$

Vertical bars, not scaled, indicate the positions of expected spectral interference lines. E3 spectrometer, column accelerating voltage: 15 kV, electronic beam current: 300 nA; diameter: 5 μm; step: 0.01 mm; integration time: 4 s. SCA windows optimized using differential mode. Horizontal bars indicate suitable background positions (see text).

set region. La (Lα1, Lα2), Nd LL and first-order lines S Kα1,2, Kα+, Kα3 and Kα4 (Figure 4) interfere on the positive off-set region. Ce and La interference lines can be minimized with PHA. La and Ce orthophosphates (Jarosewich and Boatner, 1991) usually used as REE standards, contain Pb impurities in variable amounts (Donovan et al., 2003), and may be used to analyze interference effects of these element over the Pb Mα line. In Figure 4, REE glass specter (with 3.21, 3.65, 3.79, and 1.81 wt% of La, Ce, Pr, and Y, respectively, acc. Drake and Weill, 1972) is showed for comparison.

Interferences of the Th Mζ and S K lines can be empirically avoided, but the Y Lγ lines, and the spectrum complexity in the region of interest stimulates continuous radiation modeling to interpolate background values (e.g., Geisler and Schleicher, 2000; Pyle et al., 2005). This is a desirable procedure when the measured Pb amounts are very low, as for zircon dating, and almost obligatory if Au coating was chosen (Jercinovic and Williams, 2005). If the corrections of Y and Th interferences over Pb Mα were relatively high, the Pb Mβ line, with only minor U Mζ interference, should be selected (Scherrer et al., 2000). Of course, this late choice must be made for Pb analysis in xenotime and common thorite. A suitable background off-set in negative side could be chosen in a narrow region

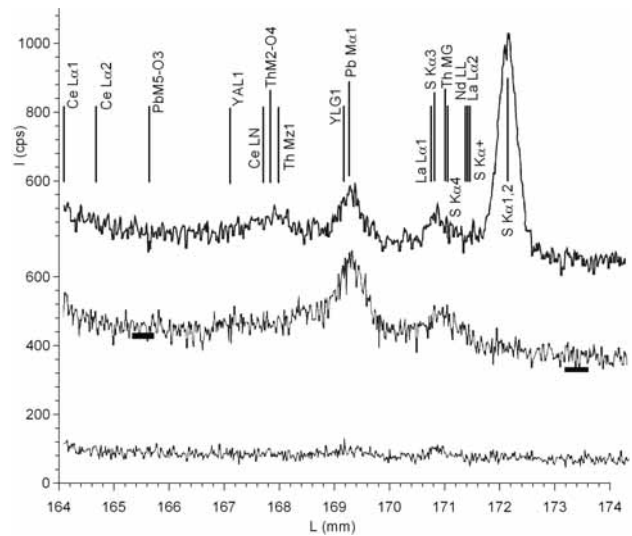


Figure 4. WDS step scanning for the region of interest to Pb Mα in monazite of biotite monzogranites from Piedade (PD-562 sample, upper) and Areia Branca (APAB-956 sample, intermediate) plutons; and in REE3 glass (Drake and Weill, 1972). Intensities were smoothed (acc. caption in Figure 3). Vertical bars, not scaled, indicate the positions of expected spectral interference lines. E4 spectrometer, column accelerating voltage: 15 kV, electronic beam current: 300 nA; diameter: 5 μm; step: 0.01 mm; integration time: 4 s. SCA windows optimized using differential mode. Horizontal bars indicate suitable background positions (see text).

between Ce L α 2 and Th M ζ , in the neighborhood and, ideally, before PbM5-O3 line (Figure 4), while, in positive side, after S K α 1,2line. -3.65/+3.9 values are often used in our lab. The -3.65 offset position is critical (e.g., Jercinovic, Williams, Lane, 2008), a bypassed situation in our procedure (acc. following item). In the positive side, the best position depends on S amount, and selected value is optimized to S values < 0.2 wt%. Of course, such off-set is not suitable if PbS was chosen as Pb standard. The linearly interpolate values from such nonsymmetrical off-sets, corrected for Th interference, are overestimated in ca. 0.14%, equivalent to less than ca. 15 ppm in the measured Pb abundance.

For a consistent correction of YL γ interference over Pb M α , the former must be determined with the due accuracy. Y L α (L = 70.23 mm) characteristic position with TAP crystal is in a region with marked continuous curvature, that presents important Nd L β 1-4 (n = 3) interference on the characteristic and background positions, P K α and Pr L β 2-15 as well Y L β 1 (n = 1) on the negative side, and Ce L β 2-15 (n = 1), Sm L α 1 (n = 3), Si K α and Ca K α (n = 1). Sr L β lines interfere on both characteristic and background region of interests, and they could not be filtered with the PHA. Small background off-sets were chosen in order to compensate these effects based on the scanning of various natural and synthetic standards (acc. Table 1).

Secondary fluorescence effects may occur in boundary zones between different minerals and should be critical when most external rim zones of a crystal are to be analyzed in rock sections (e.g., Goldstein et al., 1992; Reed, 1993, 1996). Jercinovic and Williams (2005) show detectable amounts of K, due to secondary fluorescence induced by LREE radiation into neighboring K-feldspar, up to a 10 - 15 μ m away from the contact with this mineral, and that the primary radiation intensity is kept through distances within monazite up to ca. 20 μ m. Similar effects could also affect the region of interest to Y analysis in TAP crystals. Analysis of likely effects due to compositionally largely contrasted domains within monazite crystals would be desirable.

Spectral interference contours and corrections

Taking into account that peak shape and position do not change, and that the X-ray intensity vary linearly, interferences affecting both the characteristic and background regions of interest for a reference element, typically of Th M ζ 1, 2 over Pb M α , and to a lesser degree, S K family over Pb M α , and Th M γ over U M β , could be minimized, at least, with empirical procedures (e.g., Reed, 1993). We used such an approach at times but, currently, the corrections of Th over U and Th over Pb and Y are numerically made, as described in the following.

On the negative Pb M α off-set background position, quantification is critical due to Pb M5-O3 and Th M ζ 1, 2 interferences, and Jercinovic, Williams and Lane (2008), among others, argue that linear interpolation is not suitable. However, considering that the Pb M α and M5-O3 line intensities hold a constant relation between standard and sample, for the same analytical condition, any contribution of latter will be canceled in k ratios (ratio between sample and standard intensities). In its turn, the effects of Th M ζ 1, 2 lines are corrected (acc. below) considering both the measured intensities over characteristic and background off-set. Its effect must also cancel.

The simplest formulations for interference corrections (e.g., Åmli and Griffin, 1975; Roeder, 1985) correct the measured intensity (cps/nA) taking into account empirical factors. In a general way, the corrected intensity of an A element ($I(A)_{cor,Samp}$) suffering interference of a B element is as follows:

$$I(A)_{cor,Samp} = I(A)_{meas,Samp} - I(B)_{meas,Std,posA} \times \frac{I(B)_{meas,Samp}}{I(B)_{meas,Std}} \quad (4)$$

where $I(B)_{meas,Std,posA}$ is B intensity at the A syntonization position, measured in a standard without the A element.

A correction to matrix effects is needed, however, because sample and standard compositions are much different. For instance, the (ZAF) factors, calculated with the PROZA program, for Th M and Y L line intensities in the ThSiO₄, YALG, and YPO₄ standards are 1.1548, 1.3363 and 1.1603, while in a typical monazite they vary between 1.30 and 1.32, and between 1.50 and 1.52, respectively. The corrections applied in our lab are based on the proposals of Donovan, Snyder and Rivers (1993) and Fialin, Outrequin and Staub (1997) as following:

$$I(A)_{cor,Samp} = I(A)_{meas,Samp} - I(B)_{meas,Std,posA} \times \frac{C_{(B)}^{Samp}}{C_{(B)}^{Std}} \times \frac{(ZAF)_{(B)}^{Samp}}{(ZAF)_{(B)}^{Std}} \quad (5)$$

The F factors of the L and M secondary lines are not known, and are approximated to the primary line value or alternatively to a unit. The possibility of a Y L γ peak position shift in YALG in relation to monazite (Jercinovic and Williams, 2005) may contribute to worse the correction results if such standard was used.

Numerical corrections should be introduced into the iterative procedure for matrix effects correction. The Age_Cor program, developed as an Excel spreadsheet, does these corrections on-line. However, arising out of difficult of interface with the Voyager PROZA program, our

corrections are applied just to the final results. As the U and Pb_T intensities are small, this procedure is appropriate.

Detection and quantification limits

The detection limit of an element in a sample for a confidence level defined by the critical coefficient z_c can be written as (e.g., Wittke, 1998):

$$C_{DL,Samp} = \frac{z_c \times \sqrt{2 \times I_{B,samp} \times T_{B,Samp}}}{K_{Std} \times T_{B,Samp}} \quad (6)$$

where C_{DL} is given in % element weight, I_B and T_B are intensity (cps) and counting time for the background radiation in sample, respectively; K is the intensity measured per unit of element concentration (cps/% weight) in the standard. Taking into account the standard matrix effect corrections (ZAF), it can be written:

$$K_{Std} = \frac{I_{P,Std} - I_{B,Std}}{C_{Std} \times (ZAF)_{Std}} \quad (7)$$

where I_p is the measured peak intensity. Combining equations:

$$C_{DL,Samp} = \left(\frac{C_{Std} \times (ZAF)_{Std}}{I_{P,Std} - I_{B,Std}} \right) \times z_c \times \sqrt{2 \times \left(\frac{I_{B,Samp}}{T_{B,Samp}} \right)} \quad (8)$$

The detection limit expresses the lowest abundance value for an element in a given sample that is statistically significant. In the practice, it is interesting to know the minimal *measurable* elemental amount. Potts (1996) defines a quantification limit with $z_c = 10$.

Figure 5 illustrates the variation of the Pb detection limit to some confidence intervals in dependence of counting times to our E4 spectrometer. In monazite, for a 95% confidence level, the Pb detection and quantification limits for the applied analytical conditions are about 80 and 400 ppm, respectively. Detection limit for Th and U is about 90 ppm.

DATA ANALYSIS, TREATMENT AND PRESENTATION

A monazite dating procedure should generate as complete as possible point analysis. Good analyses should result in suitable oxide totals and, importantly, in compatible cationic proportions. The REEs should also show coherent patterns.

The precision and accuracy of the obtained ages put limits for interpretations. Thus, evaluation of the data should be well established. These topics will be discussed in the next.

Chemical age models

Th-U-Pb_T ages can be calculated through point or isochronic models, which are reviewed. Usually, age-determining elements are expressed in oxide or element % wt. The use of atomic proportions seems to be more logical in isochrones, however.

If the amount of Pb₀ is known, insignificant or null, point t age can be calculated by iteration of Eq. 1 on each (Th, U, Pb_T) measured and corrected values, as applied by Montel et al. (1996). The exponential terms of this equation can be expanded to potency series according to Taylor-Maclaurin series:

$$\exp(\lambda t) = 1 + \lambda t + \frac{(\lambda t)^2}{2!} + \frac{(\lambda t)^3}{3!} + \dots \quad (9)$$

The first t value can be obtained by the first degree expansion as:

$$t_{Ma} \approx \frac{22,500 \times (Pb_T - Pb_0)}{Th + 3.14 \times U} \quad (10)$$

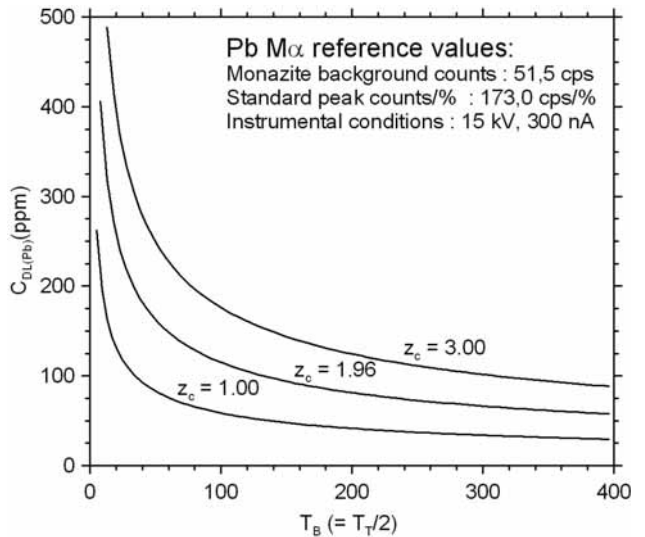


Figure 5. Variation of Pb detection limit as a function of background counting times (T_B) and of the critical z_c coefficient for instrumental conditions indicated in E4 spectrometer.

This value is a first approximation for Pb_T and initiates iterative process on Eq. 1 up to a desirable convergence. The Age_Cor program calculates on-line point ages after accomplishing corrections for spectral interferences following this procedure.

A set of N isochronic points with near normal distribution (as for N ≥ 30) defines a population, whose average age is calculated by weighted averaging, considering the inverse of the variance determined to each age value (see below).

If Pb₀ is constant, Eq. 1 is a plane equation in Th-U-Pb space, and can be written as:

$$x \times Th + y \times U - Pb_T + Pb_0 = 0 \quad (11)$$

where:

$$x = K^{Th} \times (\exp(232\lambda_{Th}t) - 1), \text{ and}$$

$$y = K^{U8} \times (\exp(238\lambda_U t) - 1) + K^{U5} \times (\exp(235\lambda_U) - 1)$$

A (Th, U, Pb_T) data set representative of isochronic points with suitable dispersion in the space defines this plane. The coefficients (x, y, Pb₀) can be calculated with normal methods, as proposed by Rhede, Wendt and Förster (1996). The x and y coefficients give independent Th-Pb and U-Pb ages, respectively. The Th-Pb age is expressed as:

$$t_{Th-Pb} = \frac{1}{232\lambda_{Th}} \times \ln(1 + 1.115567 \times x) \quad (12)$$

where the factor 1.115567 transforms element wt % to atomic % quantities. Accordingly, the y coefficient gives the U-Pb age.

U abundances can be transformed in equivalent Th (Th_{eq}) amounts, it means, Th amount that generates the same radiogenic Pb than that one originated by the measured U for a certain time interval. Defining Th* = Th_{meas} + Th_{eq} the U term can be eliminated in Eq. 11, turning it a linear equation in Th* and Pb_T coordinates:

$$xTh^* - Pb_T + Pb_0 = 0 \quad (13)$$

This formulation, originally expressed in % wt. oxide, is the base of CHIME method (Suzuki and Adachi, 1991). Equalizing the right terms of Eq. 1, we can write:

$$\frac{Th^* = Th_{meas} + U_{meas} \times [K^{U8} \times (\exp(238\lambda_U t) - 1) + K^{U5} \times (\exp(235\lambda_U t) - 1)]}{K^{Th} \times (\exp(232\lambda_{Th} t) - 1)} \quad (14)$$

and calculate Th* to a specific t value for any measured (Th, U) pairs. Similarly, a U* = U_{meas} + U_{eq} quantity could be defined and calculated for high U/Th minerals as unaninite and zircon.

The x angular coefficient of the fitted line allows calculating t age, according to Eq.12, while the intercept on the Th* axis gives a Pb₀ estimative. Th* e t are obtained trough successive iteration on equations 13 e 14.

When the data dispersion does not allow obtaining appropriate precision for x coefficient, the isochron could be drawn to the origin (Th*, Pb_T)₀ = (0 ± 2σ, 0 ± 2σ), e.g., Cocherie et al. (1998), a procedure that introduces a certain bias in the uncertainty of the angular coefficient.

An alternative isochronic model was developed by Cocherie and Albarede (2001). Assuming Pb₀ = 0, and dividing Eq. 11 by Pb_T, we obtain:

$$x \times \frac{Th}{Pb_T} + y \times \frac{U}{Pb_T} - 1 = 0 \quad (15)$$

A linear Th/Pb_T = f (U/Pb_T) type equation with angular coefficient given by:

$$y/x = - \frac{[(K^{U8} \times (\exp(238\lambda_U) - 1)) + (K^{U5} \times (\exp(235\lambda_U) - 1))]}{K^{Th} \times (\exp(232\lambda_{Th}) - 1)} \quad (16)$$

where the K constants were defined in Eq. 1. The intercepts on the Th/Pb_T and U/Pb_T axis allow the calculation of independent Th-Pb and U-Pb ages, respectively. The Th-Pb age is given by:

$$t_{Th-Pb} = \frac{1}{232\lambda_{Th}} \times \ln \left(1 + \frac{1}{K^{Th} \times (Th/Pb_T)_0} \right) \quad (17)$$

where (Th/Pb_T)₀ is the intercept on the Th/Pb_T axis. The t_{U-Pb} age may be obtained with the (U/Pb_T)₀ term. When line fits are appropriated, and Th-Pb and U-Pb ages are concordant, a probable age can be calculated more precisely since the weighted averages of Th/Pb and U/Pb ratios and error envelopes, the late defined, for instance, by the Isoplot program (Ludwig, 2003).

Results obtained with point method model are significant when Pb₀ ≅ 0, which seems to be a general rule in natural monazite and xenotime. The main disadvantages of isochronic models are: (1) the assumed premise that the used data represent isochronic points indeed, and (2) Th and/or U vary enough for good fits. On the other hand, ages depend only on plane and/or line slopes, so, if systematic errors or a combination of these errors add or subtract

constant Th, U and/or Pb_T amounts, they do not influence on the calculated ages.

The Age_Mona Excel spreadsheet has been developed, with collaboration of Guilherme A. R. Gualda, to calculate ages and generate parameters for age calculations according to all these models. Point ages and their uncertainties are calculated both through Monte Carlo modeling and iteration of Eq. 1. A modification settled up for isochronic calculations is the use of atomic fractions rather than wt%, which allows to send the obtained data to the Isoplot program automatically, to calculate isochronic and weighted average ages. Isoplot is very versatile, and has become the most used program in geochronology.

Result evaluation: precision and accuracy

Errors, quantifiable or not, can be introduced in various stages, beginning with issues related to sample representativeness and preparation, until the analysis and data treatment. Excluding the first ones and errors related to inappropriate equipment operation, the final error includes random error contributions related to X-ray generation and pulse integration processes, which affect precision (i.e., reproducibility of results), and systematic errors that depend on analytical and instrumental factors, and affect accuracy (that is, how much a given value approaches to the real value). Scherrer et al. (2000), Pyle et al. (2005), and Lisowiec (2006) examine in detail the main factors that affect method accuracy and precision.

Error propagation associated to analytical and data treatment steps, up to the final age obtaining, can be done with the classical Bevington (1969) formulation to uncertain propagation of x₁, x₂, ... x_n primary variables into a secondary y variable described by a y = f(x₁, x₂, ... x_n) function:

$$\sigma_y^2 = \sum_{i=1}^n \left(\frac{\partial y}{\partial x_i} \right)^2 \times \sigma_{x_i}^2 + \sum_{i=1}^n \left(\frac{\partial y}{\partial x_i} \times \frac{\partial y}{\partial x_j} \right) \times s_{x_i x_j} \quad (18)$$

where σ² and S represent variance and covariance, respectively. S is null when primary variables are independent, with not correlated errors.

The Voyager system uses Poisson statistics to evaluate uncertainty associated with analytical determinations. The standard deviation and relative error propagated to the k-ratios (ratio between the measured cps/nA intensities for samples and standards), are given by:

$$\sigma_k = k \times \sqrt{\frac{\sigma_{Sp}^2}{I_{Sp}^2} + \frac{\sigma_{Std}^2}{I_{Std}^2}} \quad \Leftrightarrow \quad \varepsilon_k = \frac{\sigma_k}{k} \quad (19)$$

This procedure does not consider systematic errors, thus real uncertain are underestimated (acc. Goldstein et al., 1992). Lisowiec (2006) demonstrates that the uncertainties assumed in some publications are actually lower than real, with implications for the presented interpretations (see also Spear, Pyle, Cherniak, 2009).

Given the unavailability of specific standards for monazite determination accuracy, a 2% arbitrary value is attributed to systematic errors (ε_S), taking into consideration matrix effect correction errors (1 - 2%, e.g., Reed, 1996), and internal statistic tests with conventional standards. So, the relative error in Th, U and Pb_T is calculated to a 95% confidence level as:

$$\varepsilon_T = \sqrt{\varepsilon_k^2 + \varepsilon_S^2} \quad (20)$$

The higher contributions to uncertainty in common monazite come from counting statistic to U and Pb_T and systematic errors to Th.

Measured U and Pb_T intensities incorporate contributions due to Th, and Th + Y overlaps, respectively, so that the actual uncertainty due to counting statistics are higher than the calculated ones. Interference correction procedures introduce also additional uncertain. Pyle et al. (2005) present a wide formulation to evaluate intensity uncertainty due to interferences, showing that the effect is relatively unimportant. Age_Cor program calculates relative intensity errors corrected by error propagation in Eq. 5 through the approximation:

$$\varepsilon(I(A)_{cor,Samp}) = \frac{\left[(I(A)_{meas,Samp} \times \varepsilon(I(A)_{meas,Samp}))^2 + (I(B)_{meas,Samp,posA})^2 \times (\varepsilon(I(B)_{meas,Std,posA})^2 + \varepsilon(C(A)_{Samp}))^2 \right]^{1/2}}{I(A)_{Samp}} \quad (21)$$

which is valid when:

$$\frac{(ZAF)_{(B),Std}}{C_{(B),std} \times (ZAF)_{(B),samp}} \approx cte$$

Next, the program evaluates uncertainties due to point ages. At first, a normal distribution is obtained through Monte Carlo modeling, which defines a population average and uncertainty for a 95% confidence. Secondly, the

numerical propagation of the Th, U, and Pb_T uncertainties is done applying the Bevington (1969) formulae, assuming S = 0, on the second degree Taylor-Maclaurin expansion of the age equation, which can be written as:

$$a \times t^2 + b \times t + c = 0 \quad (22)$$

where:

$$a = \frac{1}{2} \times \left[\frac{(^{232}\lambda_{Th})^2 \times K^{Th} \times Th + (^{238}\lambda_U)^2 \times K^{U8} \times U + (^{235}\lambda_U)^2 \times K^{U5} \times U}{(^{232}\lambda_{Th})^2 \times K^{Th} \times Th + (^{238}\lambda_U)^2 \times K^{U8} \times U + (^{235}\lambda_U)^2 \times K^{U5} \times U} \right]$$

$$b = ^{232}\lambda_{Th} \times K^{Th} \times Th + ^{238}\lambda_U \times K^{U8} \times U + ^{235}\lambda_U \times K^{U5} \times U$$

$$c = Pb_0 - Pb_T$$

This expansion is an excellent approach when (λt) < ca. 0.3, and the uncertainties obtained with this method match well Monte Carlo results for most of the compared situations.

Simple error analysis reveals that the propagated uncertainties to ages depend mainly on the uncertainties associated with Pb_T determinations, which quickly increase as the Pb_T amounts decrease. If Pb₀ ≅ 0, the Pb_T amounts depend only on Th and U abundances and the elapsed time. Then, simulations with variable Th and/or U concentrations and ages allow a good estimative of the expected errors on age calculations as functions of Th* and elapsed time as well as evaluating applicability limits of the method (Figure 6). As an example, this figure shows that the expected relative errors (95% confidence) for monazite with Th* = 8 wt% are about 25, 5.5, 3.5 and 2.0% for ages of 0.1, 0.5, 1.0 and 2.0 Ga, respectively. So, point age results will be close to 100 ± 25, 500 ± 28, 1,000 ± 35 and 2,000 ± 40 Myr. The diagram highlights also that, as the Th* values increase, the applicability of the method extends to samples each time young.

The propagated standard error to the population average (σ_p) is given according to Bevington formulation. Given S = 0:

$$\sigma_p^2 = \frac{1}{\sum_{i=1}^n \frac{1}{\sigma_i^2}} \quad (23)$$

where σ_i is the standard error of each determination. As a consequence, Figure 6 can also be used to evaluate the necessary minimal number of determinations to reach a desirable average error.

The laboratory procedure is more careful in dealing with propagated errors when compared to others (e.g., Pyle

et al., 2005; Cocherie and Albarede, 2001) that possibly underestimate the actual errors (acc. Lisowiec, 2006). On the average, the used approach results in errors about two times greater than the ones obtained by the later author.

The accuracy of monazite dating procedures is checked by analyzing simultaneously reference samples with well-known isotopic ages. Monazite crystals from granites (280 - 620 Myr), and medium- to high-grade metapelites (625 - 780 Myr), rocks with homogenous structure and texture, were chosen as our internal standards, whose representative compositions are presented in Table 2. Isotopic and chemical dating results for these standards are compared in Figure 7. The observed differences are within the calculated errors in all cases.

Despite the consistence of our results, it is noteworthy that good monazite standards, with variable and well-defined compositions and ages, are necessary, to compare analytical and data treatment procedures available in the literature, and to define better the accuracy of the EPMA results.

SAMPLING AND ANALYSIS PRACTICAL PROCEDURES

Common preparations are polished thin sections and grain mounts. Thin sections work better, as they allow identifying the textural context of analyzed crystals.

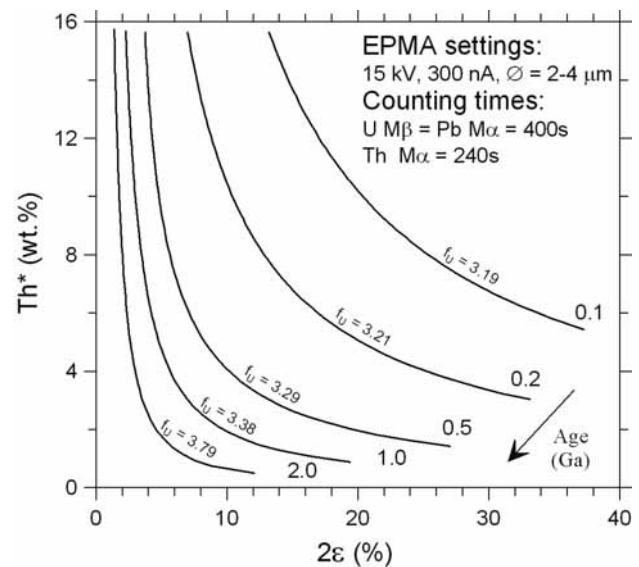


Figure 6. Dependence of the expected standard errors for point ages obtained through numerical propagation, for a confidence level of 95%, as a function of measured Th* quantities and ages, for the indicated instrumental conditions. f_U is a conversion factor to transform measured U (U_{meas}) into Th (Th_{eq}) equivalent. $Th^* = Th_{meas} + f_U \cdot (U_{meas})$, and $f_U \approx 3.17 + 0.21 \cdot t + 0.05 \cdot t^2$ (t in Gyr).

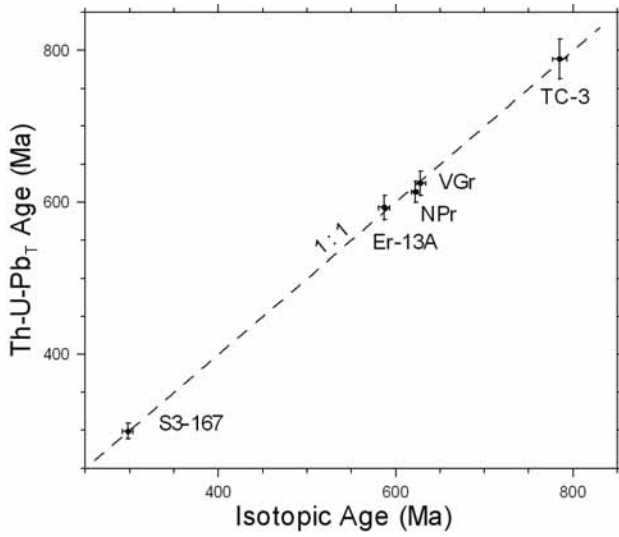


Figure 7. Comparison between obtained ages through isotopic and chemical methods for the reference samples used in our laboratory. Samples: Calde biotite monzogranite (K-Ar in biotite, Leite et al., 2005); Natividade biotite monzogranite (U/Pb in monazite, ID-TIMS, Janasi et al., 2003); Nazaré Paulista garnet leuco-monzogranite (U/Pb in monazite, ID-TIMS, unpublished data); Varginha garnet-kyanite granulite (VGr, U/Pb in monazite, ID-TIMS, Vlach and Gualda, 2000); Juscelândia garnet-silimanite gneiss (TC-3, U/Pb in zircon, SHRIMP, Vlach and Correia, 2001).

Table 2. Representative WDS analyses, cation proportions, point ages, and related errors for some monazite crystals used as reference samples in our EPMA Lab. **c** = core; **i** = intermediate zone; **r** = rim; **na** = not analyzed; **bd** = below detection limit.

Sample	Em-013A (granite)			S3-167 (granite)			TC-3 (gneiss)			VGr (granulite)		
Grain	15	15	15	4	6	6	2	2	2	1	2	2
Point ID	14, i	1,r	4, c	2,c	4,i	8,r	3, i	2,i	10,r	1,i	2,c	2,r
Oxides (wt.%)												
SiO ₂	1.84	0.27	0.03	0.42	0.16	0.37	1.21	1.16	0.55	0.22	0.23	0.23
ThO ₂	13.78	7.17	2.92	10.53	6.78	4.97	8.93	8.89	5.52	4.56	4.79	5.75
UO ₂	0.643	1.009	1.047	1.424	2.581	0.111	0.120	0.125	0.222	0.19	0.16	0.17
Al ₂ O ₃	bd	0.04	0.07	0.02	bd	bd	bd	bd	0.02	bd	0.03	bd
La ₂ O ₃	11.55	13.64	15.60	9.68	10.54	15.39	14.74	14.35	15.83	13.76	15.21	14.68
Ce ₂ O ₃	24.38	27.51	30.06	23.74	24.22	30.45	29.86	29.92	31.86	30.12	31.26	30.52
Pr ₂ O ₃	2.66	2.91	2.97	2.96	2.98	3.16	3.10	3.02	3.06	3.38	3.25	3.29
Nd ₂ O ₃	10.50	10.30	10.38	10.88	11.06	11.24	10.73	11.07	11.26	12.72	11.83	11.90
Sm ₂ O ₃	2.16	2.02	1.60	2.65	2.62	1.45	1.23	1.34	1.19	2.06	1.56	1.71
Gd ₂ O ₃	1.62	1.37	1.14	1.81	2.11	0.99	0.63	0.63	0.26	1.28	0.67	0.85
Tb ₂ O ₃	0.14	0.18	0.09	na	na	na	bd	bd	bd	bd	bd	bd
Dy ₂ O ₃	0.52	0.56	0.55	0.89	1.18	0.31	0.11	0.08	0.07	0.24	0.08	0.13
Er ₂ O ₃	0.06	0.10	0.14	na	na	na	bd	bd	bd	bd	bd	bd
Yb ₂ O ₃	0.12	0.10	0.11	0.10	0.10	0.07	0.05	0.07	0.06	0.08	bd	bd
Y ₂ O ₃	1.36	1.46	1.52	2.33	2.81	0.90	0.21	0.21	0.05	0.44	0.07	0.18
FeO	bd	bd	bd	0.06	0.25	bd	bd	bd	0.02	bd	bd	bd
CaO	1.28	1.54	0.83	2.18	1.84	0.78	0.76	0.76	0.80	0.81	0.84	0.83
PbO	0.402	0.270	0.158	0.188	0.194	0.067	0.322	0.311	0.211	0.14	0.14	0.17
P ₂ O ₅	27.12	30.09	30.48	29.60	30.09	29.66	28.32	28.54	29.74	29.20	29.50	29.70
Sum	100.14	100.52	99.72	99.47	99.51	99.91	100.30	100.47	100.71	99.20	99.62	100.10

(cont.)

Table 2. (continued)

Sample	Em-013A (granite)			S3-167 (granite)			TC-3 (gneiss)			VGr (granulite)		
Grain	15	15	15	4	6	6	2	2	2	1	2	2
Point ID	14, i	1, r	4, c	2, c	4, i	8, r	3, i	2, i	10, r	1, i	2, c	2, r

Cation proportions (on the basis of 16 O)

Si	0.296	0.042	0.005	0.066	0.024	0.058	0.192	0.184	0.086	0.035	0.036	0.036
Th	0.505	0.254	0.104	0.377	0.241	0.178	0.323	0.321	0.196	0.165	0.173	0.206
U	0.023	0.035	0.036	0.050	0.090	0.004	0.004	0.004	0.008	0.007	0.006	0.006
Al	-	0.008	0.012	0.004	-	-	-	-	0.003	-	0.006	-
La	0.686	0.783	0.896	0.561	0.607	0.892	0.865	0.839	0.912	0.809	0.888	0.853
Ce	1.437	1.567	1.713	1.365	1.385	1.752	1.739	1.736	1.822	1.759	1.812	1.761
Pr	0.156	0.165	0.169	0.169	0.170	0.181	0.179	0.175	0.174	0.196	0.187	0.189
Nd	0.604	0.572	0.577	0.610	0.617	0.631	0.609	0.627	0.628	0.724	0.669	0.670
Sm	0.120	0.108	0.086	0.143	0.141	0.079	0.067	0.073	0.064	0.113	0.085	0.093
Gd	0.086	0.070	0.059	0.094	0.109	0.051	0.033	0.033	0.014	0.068	0.035	0.045
Tb	0.007	0.009	0.005	-	-	-	-	-	-	-	-	-
Dy	0.027	0.028	0.028	0.045	0.059	0.016	0.006	0.004	0.004	0.012	0.004	0.007
Er	0.003	0.005	0.007	-	-	-	-	-	-	-	-	-
Yb	0.006	0.005	0.005	0.005	0.005	0.004	0.002	0.003	0.003	0.004	-	-
Y	0.117	0.121	0.126	0.195	0.233	0.075	0.018	0.017	0.004	0.037	0.006	0.015
Fe	-	-	-	0.008	0.033	-	-	-	0.002	-	-	-
Ca	0.220	0.256	0.139	0.367	0.308	0.130	0.129	0.129	0.134	0.138	0.142	0.140
Pb	0.017	0.011	0.007	0.008	0.008	0.003	0.014	0.013	0.009	0.006	0.006	0.007
P	3.695	3.963	4.017	3.937	3.979	3.945	3.814	3.829	3.933	3.942	3.954	3.963
Sum	8.008	8.004	7.989	8.006	8.090	7.999	7.999	7.991	7.996	8.017	8.009	7.991

Th, U, and Pb_r concentrations (ppm), point ages and standard errors (95%)

Th	121070	63040	25700	92570	59550	43660	78460	78120	48530	40074	42095	50490
SE	2485	1320	581	1920	1253	933	1627	1620	1028	852	890	1440
U	5670	8890	9230	12550	22755	975	1060	1100	1960	1640	1437	1498
SE	165	220	226	287	482	111	112	112	117	124	123	124
Pb	3730	2510	1470	1740	1800	625	2990	2890	1960	1300	1290	1560
SE	125	103	95	96	97	80	116	115	98	95	94	98
Age (Ma)	593	604	583	293	304	298	806	781	786	635	612	625
SE	26	32	51	22	21	57	40	40	52	58	60	52

However, sampling is more reduced and occasional when compared to grain mounts. In our lab, two or three thin sections *per* sample are prepared, for which identified (or suspected) crystal coordinates are recorded by Digimax automatic stage. Runs for Th-U-Pb_T dating are performed in the lab in weekly periods entirely dedicated to.

Transmitted and reflected light and backscattering electron microscopy

Mineral paragenesis and optical properties (e.g., Chang, Howie, Zussman, 1998) allow identifying monazite and contrasting it with zircon and/or xenotime under transmitted and reflected light microscopy in most cases. Monazite typically presents yellow-orange light absorption, cleavages and inclined extinction in (100) section. Zonality and metamictization patterns are absent, but it generates pleochroic halos larger than zircon or, even, xenotime. Under reflected light, monazite does not show the zonal structure and internal reflections, typical of most common zircon crystals. Doubtful minute crystals are easily solved with EDS or BSE images in a couple of seconds. Importantly, dating of very small crystals, < ca. 40 μm, should be avoided due to their high susceptibility to bordering effects.

BSE-Compo images are very useful to identify contrasted compositional domains within monazite, not detected under conventional light microscopy or CL images. Typical monazite compositions present average atomic (\bar{Z}) numbers between 38 and 42, well higher than most common accessories (zircon, xenotime etc.). A $\Delta\bar{Z}$ of 0.6-0.7 gives a difference about 1% in the backscattering coefficient (e.g., Reed, 1996), easily detected in good quality images. High resolution, equalized images, allows contrasting domains with even lower $\Delta\bar{Z}$. Monazite can contain, in addition to Pb, minor or trace amounts of S, Sr, Mn, Fe, Al, F, and (OH), among others (e.g., Chang, Howie, Zussman, 1998). The main compositional variations are described by brabantite, [Ca(Th,U)][REE]₂, huttonite, [Si(Th,U)][(REE)P]₁, and the single Y[REE]₁ substitution vectors (e.g., Förster, 1998). All of them result in \bar{Z} decrease, but their combinations could compensate the effects to a variable degree.

Recent studies show that the opening and resetting of monazite chemical and/or isotope systems are mainly associated with dissolution and reprecipitation phenomena. Besides, neof ormation and overgrowth mechanisms could lead to polygenetic crystals. Importantly, Pb diffusion is not significant in continental crust environments (e.g., Seydoux-Guillaume et al., 2002, Gardés et al., 2007). Thus, some compositional variations among nonisochronic domains in crystals are to be expected, and BSE images may become exceptional guides to define analytical strategies.

Elemental calibration, result evaluation, and analyses

After tests for the presence of S (and K, if necessary) and to ensure stability under the chosen instrumental conditions, spectral syntonization, verification of SCA conditions and standard element calibration (acc. Table 1), the instrumental set-up and calibration are checked with the reference samples. Monazite from the Er-13A monzogranite (ca. 590 Myr) presents significant variations in Th, U, and Y abundances, so is preferred. The quality of results is evaluated in closing test (ca. 99 - 101 wt% oxide), and adequacy of cationic proportions: sums for Si + P, and the other cations between 3.96 and 4.04 to 32 negative charges. Once these requirements are satisfied and the difference in the calculated average Th-U-Pb_T and isotopic ages available for reference samples are less than ca. 2% relative, the procedure continues, starting analyses of desired samples. When geologically related samples are analyzed in distinct runs, readings of previously analyzed samples are repeated for comparison and data validation. These are the most time consuming steps in dating routines.

BSE imaging is performed systematically, and together with petrographic information, used for grain and point analysis selection. Point analyses are done in the assisted mode, as it allows monitoring variations in the analytical conditions and results in real time. Importantly, point-to-point ages calculated with Age_Cor program allow changing analytical strategy as convenient. The JEOL-JXA8600S machine does not have automatic focus, so the automatic analysis mode is used only for compositional/age profiles of limited extent over single crystals. About 25 - 35 determinations are obtained for each age population.

The minimum time for a complete analysis is gauged by the Pb_T and U total counting time, which is 400 s in most cases, so a complete point analysis is obtained every 10 min. Some protocols presented in literature are more complex and time-consuming (e.g., Jercinovic and Williams, 2005). Complete, precise and accurate analyses can be obtained in a fully automated, well calibrated, and stable EPMA with 5 WDS spectrometers, two of which dedicated to U and Pb, and a third for Th and P (S, K, if needed) measurements. No real gains in precision or accuracy are obtained by performing distinct runs, first to determine the chemical composition and second to measure the age-determinant elements, as suggested by Pyle et al. (2005).

Compositional maps

Maps showing age variations in monazite crystals, starting from quantitative WDS mapping of Th, U, Pb and Y, and pixel to pixel conversion of elemental intensities

in ages had been pioneering by Williams, Jercinovic and Terry (1999). The average ages of crystalline domains can be computed taking into account the age of each pixel. This procedure is very useful to illustrate the patterns within crystals with significant age variations.

Quantitative WDS mapping is little explored in our lab due to the inherent difficulty of the Voyager system. Qualitative WDS and EDS dot mapping (beam scanning) are used to highlight the main compositional variation patterns, as exemplified in the following section. Dot mapping works only for high magnifications (ca. > 500) due to beam defocusing, however.

The monazite dating procedures suggested by Jercinovic and Williams (2005) are very laborious and include several steps involving successive mapping for grain selection, age map generation, and sample coating exchange (C for Au), followed by specific point analyses. We think that a good petrographic work followed by high resolution BSE imaging and quantitative point analyses result in equivalent qualitative and quantitative informations.

CASE STUDIES

In this section three examples, which illustrate characteristics and potentials of the method, are examined. The first compares ages and errors calculated for a same data set through isochronic and point methods. The second example demonstrates the potential of BSE images to identify compositional domains and the procedure applied to identify contrasted populations with close ages in polygenetic monazite crystals, while the last illustrates EPMA data relevance to identify and decipher cases of isotopic discordance.

In Figure 8, dating results are presented for monazite of a massive inequigranular biotite monzogranite (Sample APAB-956), from the Morungaba region, São Paulo, SE of Brazil (Vlach, 1993). Monazite occurs as idiomorphic crystal (0.2 - 0.8 mm) associated with biotite, ilmenite, zircon and some apatite, interstitially to felsic minerals. Thirty-one point analyses were obtained for two crystals with thin recurrent zoning, presenting significant variations in Th (3.4 - 10.5% wt.), U (0.137 - 0.582%), and also Y (0.5 - 2.2%) contents. Four analyses with (Si + P) excess were rejected.

As expected, the calculated ages are very close (Table 3). U-Pb age calculated according to Rhede, Wendt and Förster (1996) present higher errors (50 Myr) due to higher analytical errors in U as compared to Th, and to point scattering in the space. The weighted Th-Pb and U-Pb ages average is equal to the age obtained by the CHIME method. The comparison among the isochronic and weighted average results shows, as the most important feature, contrasted age errors (ca. 16 - 22 Myr, in the first case, 6 - 8 Myr (SE), in

the second case. The latter is similar to that obtained by the Tukey's Biweight average, and a bit lower than the median (8 - 12 Myr) of the modeled Gaussian distribution. In this example, if the 2D isochron is drawn to zero, the error will decrease to some extent but the MSWD will increase. The standard deviation (SD), a measure of the dispersion of computed ages within the population, is 28 Myr.

EPMA results present great reproducibility, and the weighted average age should be chosen as the most probable population age, if the results are accurate. Of course, weighted averages converge and standard errors decrease with the number of measurements (Figure 9). This figure nicely shows that there is not a significant gain in performing a number of analyses larger than ca. 25 - 35 when the individual point-analyses have not large errors (> ca. 60 Ma).

The second example shows partial results obtained for a sillimanite-garnet-biotite gneiss (Sample EM-004B) from the Piracaia Complex, collected close to the tectonic contact between this complex and the Embu Terrain, eastern São Paulo State, SE Brazil. These gneisses had been submitted to shear deformation in greenschist facies conditions, with abundant muscovite and biotite neof ormation. Well developed xenomorphic crystals of monazite, sometimes broken and deformed, were analyzed.

The BSE image of a representative crystal (Figure 10) shows a central zone with predominantly sectorial and/or patchy zoning, with grey zones partially surrounded by an irregular and darker external border. The \bar{Z} values, calculated through averages for three analyses in internal (z1) and external (z2) zones, are 41.2 and 40.7, respectively ($\Delta\bar{Z} = 0.5$).

Point ages in the crystal core vary between ca. 610 and 650 Myr while in rim zones vary between ca. 570 and 610 Myr, suggesting the existence of two age populations. A significant overlap for the intervals of the individual errors, between 40 and 60 Myr, exists, however. Situations like this, involving component identification and deconvolution within a heterogeneous population, can be treated through mixing models (Sambridge and Compston, 1994). This was done with the Isoplot program, which incorporates a simplified algorithm, valid for normal distributions. The results indicate two statistically significant populations, one with a probable age of 627 ± 14 Myr, another with 588 ± 18 Myr, with a relative misfit close to 1.

These ages are compatible with the recorded Neoproterozoic tectonic evolution of this region (Vlach, S.R.F., in preparation) and demonstrate that Th-U-Pb_r dating of monazite allows contrasting age differences as low as ca. 30 Myr. It is worth to note that, independently of some possible inaccuracy in the obtained absolute values, the time interval recorded between the main metamorphism and the overprinted retro-metamorphism has real significance.

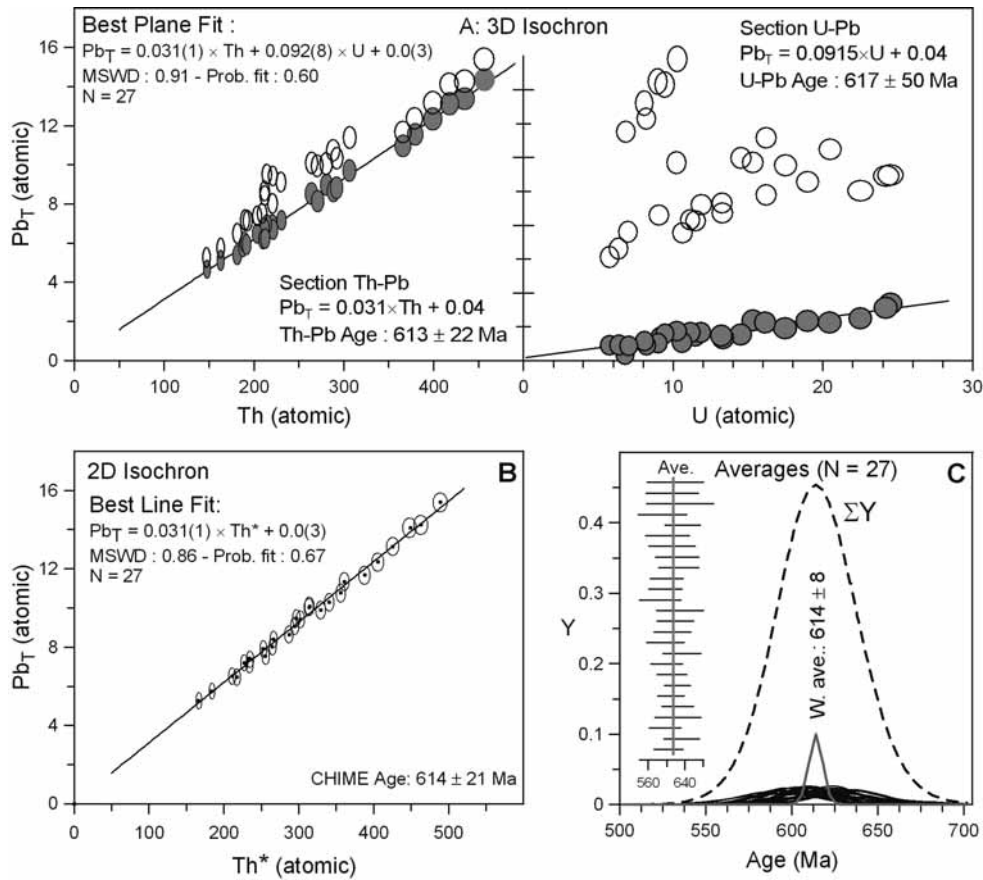


Figure 8. Comparison between computed ages and data representation schemes for isochronic and weighted averages methods (Sample APAB-956). **A.** Th vs Pb_T and U vs Pb_T sections from Th-U- Pb_T (atomic proportions) space and the best fitted Th- Pb_T and U- Pb_T isochrones. Error ellipses are projected along the fitted plain on intersection (full), and orthogonally on reference section (empty) by comparison. **B.** Th*- Pb_T cationic isochron. **C.** Gaussian probability density distributions for point ages, its sum, and the population weighted average. A bar diagram showing dispersion of individual results in relation to the weighted average is presented in the inset.

Table 3. Summary of monazite dating results for APAP-956 sample through isochronic methods and averages (SE = standard error of weighted average; SD = standard deviation of simple average).

Chemical Method	Age (Ma)	SE	MSWD	Prob. fit	SD
3D chemical isochron: Rhede, Wendt and Förster (1996), modified					
Th- Pb_T age	613	22	0.91	0.60	
U- Pb_T age	617	50	0.91	0.60	
Weighted Average	614	20			
2D chemical isochron: Suzuki and Adachi (1991), modified					
Model 1	614	21	0.86	0.67	
Model 1, to 0	611	16	0.83	0.72	
Robust fit	616	21/-23			
Robust fit, to 0	612	18			
Averages: (Montel et al., 1996; Ludwig, 2003)					
Weighted Average	614	8	0.48	0.99	28
Tukey's BiWeight	615	6			
Median	613	11/-8			

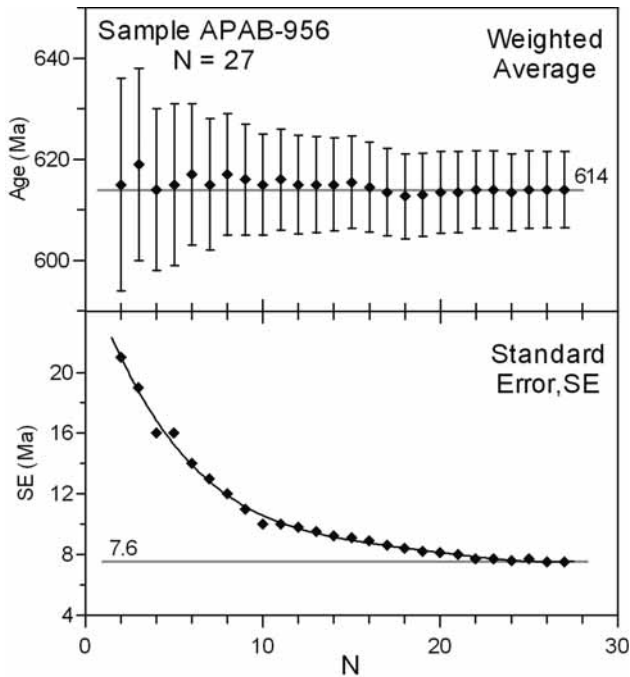


Figure 9. Variation of the calculated weighted averages and standard errors of the mean (SE) as a function of N, the number of monazite analyses considered. Data from APAB-956 biotite monzogranite. See text.

The last example comes from a biotite-garnet migmatitic gneiss (CE-118) of the São José do Campestre Massife, an Archaean nucleus of Borborema Province, Ceará state, Northeast of Brazil (Vlach and Dantas, 2001). Conventional isotopic U/Pb results (ID-TIMS) had revealed two crystal populations with contrasted ages (Figure 11): a homogeneous population, constituted by small, idiomorphic, and transparent crystals, is concordant or slight discordant and gives ca. 570 - 580 Myr; the other, formed by larger, xenomorphic, and less transparent crystals, is highly discordant, and points to an upper intercept at ca. 3.0 Gyr (Dantas et al., 1999). WDS dot-maps of a typical second generation crystal evidence contrasted zoning patterns: more or less normal for Pb and complex of Th, Y, and U. The observed patterns strongly suggest that this crystal was infilled by late solutions that replaced the primary monazite in somewhat weakened zones, by a Y-, U-, and HREE-rich and Th-poor variety.

The computed weighted average ages are ca. 2.99 ± 0.01 Gyr and 580 ± 25 Myr, respectively. This is a clear case where the observed isotopic discordance is due to the mixture of distinct fractions of chemically and isotopically contrasted domains. This is an extreme example, as discordance is very high. In general, the evolution of metamorphic terrains and related magmatism puts under relief situations whose age differences can be well smaller,

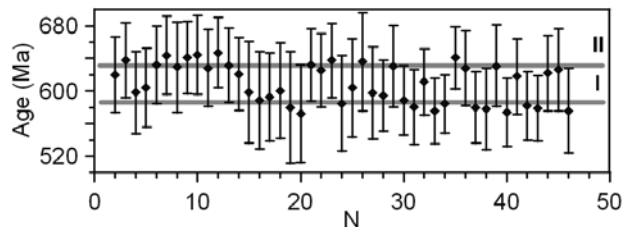
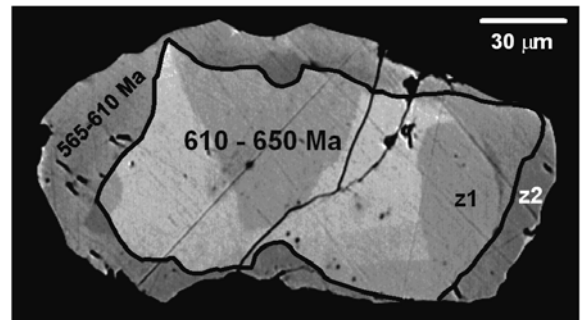
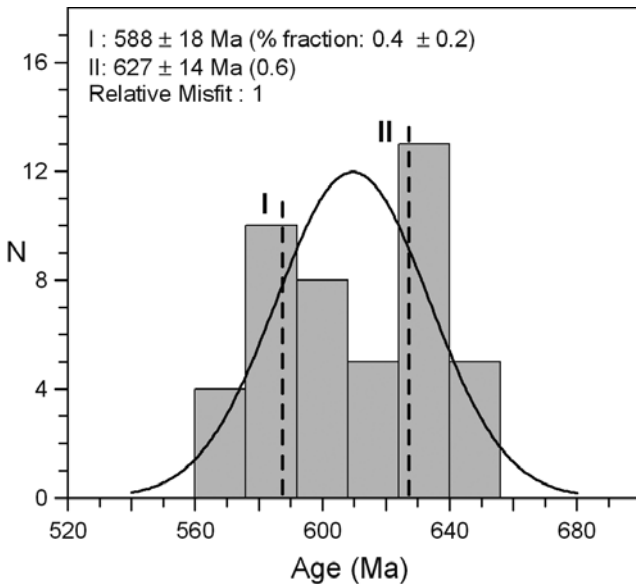
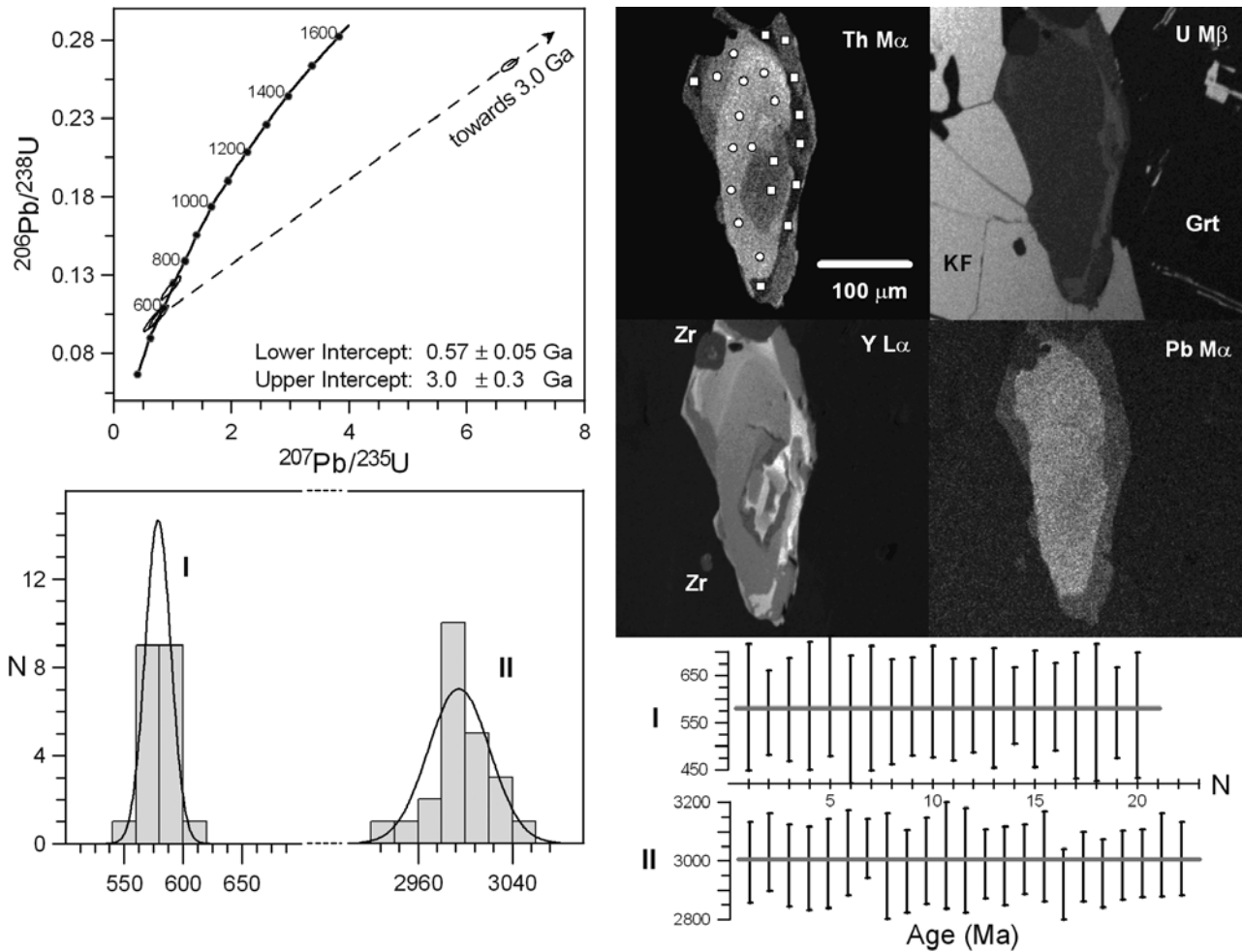


Figure 10. Dating results for polygenetic monazite in sillimanite-garnet gneiss EM-004B, and BSE image of a typical xenoblastic crystal. Unmixing age results obtained with the Isoplot program. The internal zone of crystal presents sectorial and/or patchy zoning; the youngest external zone is more irregular and shows lower backscattering coefficient. The z1 and z2 zones present ΔZ about 0.5. See discussion in text.

ca. < 100 Myr, such as in our second example. In such situations, isotopic ID-TIMS data could appear concordant or very slightly discordant, and mixing ages could be taken as crystallization ages (Vlach et al., 2002).

This example also hands out for analysis of error variation in dependence of sample composition and age. The measured Th, U e Pb_T amounts in new and old crystal zones vary from 7,000 - 25,000, 1,500 - 7,000, and 500



I: Weight Ave: 579 ± 17 Ma, MSWD: 0.1, Prob fit: 1, SD (95%) : 24 Ma, Median: 580 +5/-8 Ma
II: Weight Ave: 3,003 ± 12 Ma, MSWD: 2.7, Prob fit: 0, SD (95%): 58 Ma, Median: 2,992 +17/-10 Ma

Figure 11. Monazite dating results for the Ce-118 migmatitic gneiss. Upper left side: concordia diagram illustrating two monazite populations, a younger one, concordant or slightly discordant, and an older one, strongly discordant. Upper right side: X-ray dot maps (WDS) showing Th, U, Y, and Pb distribution in a polygenetic monazite crystal. In the U M β map, U intensities are not corrected for K K α overlap, as it is evidenced by the U high apparent intensities in potassium feldspar. Notice irregular in-fillings with abrupt contacts, well marked in the maps by increased Y and U as well as decreased Th intensities, interpreted as due to dissolution-reprecipitation processes. Pb map shows more regular concentric zoning, which partially follows the observed Th zoning. KF = potassium feldspar; Grt = garnet; Zr = zircon. Lower left side: histograms showing point age distribution for the Archaean and Neoproterozoic populations. Lower right side: bar diagrams showing point age dispersion in relation to the weighted averages (smooth thick trace). Observe that the relative age dispersion is too superior in the first case. See discussion in text.

- 900 to 14,000 - 35,000, 700 - 1,900, and 2,300 - 5,800 ppm, respectively. Point age errors are between 90 - 150 Myr for the young monazite, so a high standard error for the population weighted average, which approaches the standard deviation of the population (24 Myr, acc. Figure 11) was obtained. A higher number of analyses must be obtained in order to decrease such population error. The errors obtained for the individual points of the older population, with higher Pb_T amounts, are much smaller, and the propagated standard error to the population average is only about 11 Myr, but the relative data dispersion is higher, with an average standard deviation close to 60 Myr.

CONCLUDING NOTES

The best analytical protocol for Th-U-Pb_T monazite dating for a specific EPMA equipment is the simplest one capable to generate results with acceptable precision and accuracy, compatible with the inherent limitations of the method. Linear interpolation for the background Pb M α line quantification is a perfectly feasible solution, when the interference corrections to Th M ξ 1, 2 lines are appropriately considered.

The reproducibility of the quantitative EPMA results is excellent. The lack of specific compositional and age standards limits however a fine evaluation of the results accuracies, as well as adequate comparisons of different analytical protocols and data treatment schemes. The Th-U-Pb_T ages obtained in our microprobe lab to monazite with significant variations in Th, U, and Y abundances, are perfectly comparable with independent isotopic ages, taking into account realistic error intervals. The errors associated with each point age may be predicted as a function of Th and U amounts and the elapsed time since the closure of the chemical system. Monte Carlo modeling indicates that the weighted average age errors are underestimated when it is assumed that the instrumental errors are insignificant in relation to counting errors, thus, reported chemical ages with errors inferior to ca. < 2% should be analyzed with caution.

The average age calculation for an isochronic population starting from individual determinations, considering Pb₀ = 0, is the simplest procedure, with wide application. In most cases a number of 25 - 35 point analyses for each age population are enough, as the standard errors will not be much improved for a large analyses number, except in cases where the individual point errors are very high. Good-quality isochrones require a good dispersion of Th and/or U amounts. The 2D isochronic method can be very useful to test an analytical procedure and to test for the presence of significant Pb₀ amounts. Isochronic ages do not depend of systematic errors that add or subtract constant Th, U and/or Pb amounts.

The most relevant applications of the method are the ones involving geologic environments that favor the development of polygenetic monazite, due to its high spatial resolution. The implemented procedures allow, in favorable cases, to identify populations with very close ages, ca. 30 - 50 Myr, with adequate statistical meaning. BSE images, compositional variations, as well as geologic and petrographic features are essential informations to attribute or not geologic meaning for such age populations. Secondary fluorescence effects in crystal rims analyzed in thin sections and intracrystalline bordering zones with contrasted compositions must be carefully considered, once they potentially decrease the real spatial resolution of analysis, and could result in mixed, meaningless values.

The low Pb diffusion ratio in the monazite structure increments the method applicability significantly for the resolution of critical petrologic problems. The integration of data concerning micro-structure, chemistry, geothermometry and geochronology obtained for polygenetic monazite allows identify and correlate petrologic processes in the micro-scale, as well as estimate intensive parameters of crystallization and put them into the time scale. It represents a very significant advance for geosciences.

Completed analytical data concerning the presented examples as well as the programs developed in our microprobe lab can be obtained through request.

ACKNOWLEDGEMENTS

To the *Fundação de Amparo à Pesquisa do Estado de São Paulo* (FAPESP) for constant support for the EPMA lab from *Instituto de Geociências* of *Universidade de São Paulo*, and Proc. 95/5728-2, allowing automation system optimization. Dr. Ian Steele, from The University of Chicago, kindly supply several high quality standards over the last years. Marcos Mansueto and Paulo Molinaro gave support in routine work and sample preparation. Drs. N. Botelho and M. Macambira reviewed the original manuscript.

REFERENCES

- ÂMLI, R.; GRIFFIN, W. L. Microprobe analysis of REE minerals using empirical correction factors. *American Mineralogist*, v. 60, p. 599-606, 1975.
- BASTIN, G. F.; HEIJLIGERS, H. J. M. Progress in electron-probe microanalysis. *Materialwissenschaft und Werkstofftechnik*, v. 21, p. 216-221, 1990.
- BEVINGTON, P. R. *Data reduction and error analysis for the physical sciences*. San Francisco: McGraw-Hill, 1969. 326 p.

- BOWLES, J. F. W. Age dating of individual grains of uraninite in rocks from electron microprobe analysis. *Chemical Geology*, v. 83, p. 47-53, 1990.
- CASTAING, R. *Application of electron probes to local chemical and crystallographic analysis*. 1951. 132 f. Thesis California Institute of Technology - University of Paris. Translated by DUWEZ, P.; WITTRY, D. B., 1955.
- CHANG, L. L. Y.; HOWIE, R. A.; ZUSSMAN, J. *Rock Forming Minerals*. 2. ed. London: Geological Society, 1998. v. 5B, 383 p.
- CHERNIAK, D. J.; WATSON, E. B.; GROVE, M.; HARRISON, T. M. Pb diffusion in monazite: a combined RBS/SIMS study. *Geochimica et Cosmochimica Acta*, v. 68, p. 829-840, 2004.
- COCHERIE, A.; ALBAREDE, F. An improved U-Th-Pb age calculation for electron microprobe dating of monazite. *Geochimica et Cosmochimica Acta*, v. 65, p. 4509-4522, 2001.
- COCHERIE, A.; LEGENDRE, O.; PEAUCAT, J. J.; KOUAMELAN, A. N. Geochronology of poligenetic monazites constrained by in situ electron microprobe Th-U-total lead determination: Implications for lead behavior in monazite. *Geochimica et Cosmochimica Acta*, v. 62, p. 2475-2497, 1998.
- DANTAS, E.; Van SCHMUS, W. R.; HACKSPACHER, P.; FETTER, A. Identification of multiple orogenic/metamorphic events in polycyclic terranes; possibilities and limitations. Insights from the Borborema Province, NE Brazil. In: SIMPÓSIO NACIONAL DE ESTUDOS TECTÔNICOS, 7., 1999, Lençóis. *Anais...* Lençóis: SBG, 1999. p. 15-17.
- DONOVAN, J. J.; SNYDER, D. A.; RIVERS, M. L. An improved interference correction for trace element analysis. *Microbeam Analysis*, v. 2, p. 23-28, 1993.
- DONOVAN, J. J.; HANCHAR, J. M.; PICOLLI, P. M.; SCHRIER, M. D.; BOATNER, L. A.; JAROSEWICH, E. A re-examination of the rare-earth-element orthophosphate standards in use for electron-microprobe analysis. *Canadian Mineralogist*, v. 41, p. 221-232, 2003.
- DRAKE, M. J.; WEILL, D. F. New rare earth element standards for electron microprobe analysis. *Chemical Geology*, v. 10, p. 179-181, 1972.
- FIALIN, M.; OUTREQUIN, M.; STAUB, P. F. A new tool to treat peak overlaps in electron-probe microanalysis of rare-earth-element L-series X-rays. *European Journal of Mineralogy*, v. 9, p. 965-968, 1997.
- FÖRSTER, H. J. The chemical composition of REE-Y-Th-U-rich accessory minerals in peraluminous granites of the Erzgebirge-Fichtelgebirge region, Germany, Part I: the monazite-(Ce)-brabantite solid solution series. *American Mineralogist*, v. 83, p. 259-272, 1998.
- GARDÉS, E.; MONTEL, J. M.; SEYDOUX-GUILLAUME, A. M.; WIRTH, R. Pb diffusion in monazite: New constraints from the experimental study of Pb²⁺ ↔ Ca²⁺ interdiffusion. *Geochimica et Cosmochimica Acta*, v. 71, p. 4036-4043, 2007.
- GEISLER, T.; SCHLEICHER, H. Improved U-Th-total Pb dating of zircons by the electron microprobe using a simple new background modeling procedure and Ca as a chemical criterion of fluid-induced U-Th-Pb discordance in zircon. *Chemical Geology*, v. 163, p. 269-285, 2000.
- GOLDSTEIN, J. I.; NEWBURY, D. E.; ECHLIN, P.; JOY, D. C.; ROMIG JR, A. D.; LYMAN, C. E.; FIORI, C.; LIFSHIN, E. *Scanning Electron Microscopy and X-Ray Microanalysis: a text for biologists, materials scientists, and geologists*. 2. ed. New York: Plenum Press, 1992. 820 p.
- GRATZ, R.; HEINRICH, W. Monazite-xenotime thermometry. Experimental calibration of the miscibility gap in the binary system CePO₄-YPO₄. *American Mineralogist*, v. 82, p. 772-780, 1998.
- JANASI, V. A.; ALVES, A.; VLACH, S. R. F.; LEITE, R. J. Granitos peraluminosos da porção central da Faixa Ribeira, Estado de São Paulo: Eventos de reciclagem da crosta continental no Neoproterozóico. *Geologia USP. Série Científica*, v. 3, p. 13-24, 2003.
- JAROSEWICH, E.; BOATNER, L. A. Rare-earth element reference samples for electron microprobe analysis. *Geostandard Newsletter*, v. 15, p. 397-399, 1991.
- JENKIES, R.; DeVRIES, J. *Practical X-ray Spectrometry*. Berlin: Springer-Verlag, 1982. 189 p.
- JERCINOVIC, M. J.; WILLIAMS, M. L. Analytical perils (and progress) in electron microprobe trace element analysis applied to geochronology: background acquisition,

- interferences, and beam irradiation effects. *American Mineralogist*, v. 90, p. 526-546, 2005.
- JERCINOVIC, M. J.; WILLIAMS, M. L.; LANE, E. D. In-situ trace element analysis of monazite and other fine-grained accessory minerals by EPMA. *Chemical Geology*, v. 254, p. 197-215, 2008.
- KARIORIS, F. G.; GOWDA, K.; CARTZ, L. Heavy ion bombardment on monoclinic ThSiO₄, ThO₂, and monazite. *Radiation Effects Letters*, v. 58, p. 1-3, 1991.
- KEMPE, U. Precise electron microprobe age determination in altered uraninite: consequences on the intrusion age and the metallogenic significance of the Kirchberg granite (Erzgebirge, Germany). *Contributions to Mineralogy and Petrology*, v. 145, p. 107-118, 2003.
- KINGSBURY, J. A.; MILLER, C. F.; WOODEN, J. J.; HARRISON, T. M. Monazite paragenesis and U-Pb systematics in rocks of the eastern Mojave Desert, California, U.S.A.: implications for thermochronometry. *Chemical Geology*, v. 110, p. 147-167, 1993.
- LEITE, S. M.; VLACH, S. R. F.; AZEVEDO, M. R.; SANTOS, J. F. Idades Th-UPb_r em monazite do monzogranito de Calde, Maciço Granítico de Castro Daire (Centro de Portugal). In: CONGRESSO DE GEOQUÍMICA DOS PAÍSES DE LINGUA PORTUGUESA, 8., 2005, Aveiro. *Actas...* Aveiro: SBGq, 2005. v. 1, p. 231-235.
- LISOWIEC, N. Precision estimation in electron microprobe monazite dating: Repeated measurements versus statistical (Poisson) based calculations. *Chemical Geology*, v. 234, p. 223-235, 2006.
- LOVERING, J. F.; WARK, D. A.; GLEADOW, A. J. W.; BRITTEN, R. Lunar monazite: a late-stage (mesostasis) phase in mare basalt. *Earth and Planetary Science Letters*, v. 21, p. 164-168, 1974.
- LUDWIG, K. R. *Isoplot 3.00: a geochronological toolkit for Microsoft Excel*. Berkeley: Geochronological Center Special Publication, 2003. v. 4. 70 p.
- MARTINS, L.; VLACH, S. R. F.; JANASI, V. A. Reaction microtextures of monazite: correlation between chemical and age domains in the Nazaré Paulista migmatite, SE Brazil. *Chemical Geology*, v. 261, p. 271-285, 2009.
- MONTEL, J. M. A model for monazite/melt equilibrium and applications to the generation of granitic magmas. *Chemical Geology*, v. 110, p. 127-146, 1993.
- MONTEL, J. M.; FORET, S.; VESCHAMBRE, M.; NICOLLET, C.; PROVOST, A. Electron microprobe dating of monazite. *Chemical Geology*, v. 13, p. 37-53, 1996.
- OVERSTREET, W. C. *The geological occurrence of monazite*. Washington: U.S.G.S., 1967. 327p. (Geological Survey Professional Paper, 530)
- PARRISH, R. R. U-Pb dating of monazite and its applications to geological problems. *Canadian Journal of Earth Sciences*, v. 27, p. 1431-1450, 1990.
- PARSLOW, G. R.; BRANDSTATTER, F.; KURAT, G.; THOMAS, D. J. Chemical ages and mobility of U and Th in anatectites of the Cree Lake zone, Saskatchewan. *Canadian Mineralogist*, v. 23, p. 543-552, 1985.
- ROEDER, P. L. Electron-microprobe analysis of minerals for rare-earth elements: use of calculated peak-overlap corrections. *Canadian Mineralogist*, v. 23, p. 263-271, 1985.
- PODOR, R.; CUNEY, M. Experimental study of Th-bearing LaPO₄ (780° C, 200 Mpa): Implications for monazite and actinide orthophosphate stability. *American Mineralogist*, v. 82, p. 765-771, 1997.
- POTTS, P. J. *A Handbook of Silicate Rock Analysis*. London: Chapman Hall, 1996. 622 p.
- PYLE, J. M.; SPEAR, F. S.; WARK, D. A.; DANIEL, C. G.; STORM, L. C.. Contributions to precision and accuracy of monazite microprobe ages. *American Mineralogist*, v. 90, p. 547-577, 2005.
- PYLE, J. M.; SPEAR, F. S.; RUDNICK, R. L.; McDONOUGH, W. F. Monazite-xenotime- garnet equilibrium in metapelites and a new monazite-garnet thermometer. *Journal of Petrology*, v. 42, p. 2083-2107, 2001.
- RAPP, R. P.; WATSON, E. B. Monazite solubility and dissolution kinetics: implications for the thorium and light rare earth chemistry of felsic magmas. *Contributions to Mineralogy and Petrology*, v. 94, p. 304-316, 1986.
- REED, S. B. J. *Electron Microprobe Analysis*. 2. ed. New York: Cambridge University Press, 1993. 326 p.

- REED, S. B. J. *Electron Microprobe Analysis and Scanning Electron Microscopy in Geology*. New York: Cambridge University Press, 1996. 201 p.
- REED, S. J. B.; BUCKLEY, A. Virtual WDS. *Mikrochimica Acta*, v. 13, p. 479-483, 1996.
- REED, S. B. J.; BUCKLEY, A. Rare-earth determination in minerals by electron-probe microanalysis: application of spectrum synthesis. *Mineralogical Magazine*, v. 62, p. 1-18, 1998.
- RHEDE, E.; WENDT, I.; FÖRSTER, H. H. A three-dimensional method for calculating independent chemical U-Pb- and Th-Pb-ages of accessory minerals. *Chemical Geology*, v. 130, p. 247-253, 1996.
- SAMBRIDGE, M. S.; COMPSTON, W. Mixture modeling of multi-component data sets with application to ion-probe zircon ages. *Earth and Planetary Science Letters*, v. 128, p. 373-390, 1994.
- SCHERRER, N. C.; ENGI, M.; GNOS, E.; JAKOB, V.; LECHTI, A. Monazite analysis: from sample preparation to microprobe age dating and REE quantification. *Schweizerische Mineralogische und Petrographische Mitteilungen*, v. 80, p. 93-105, 2000.
- SEYDOUX-GUILLAUME, A. M.; PAQUETTE, J. L.; WIEDENBECK, M.; MONTEL, J. M.; HEINRICH, W. Experimental resetting of the U-Th-Pb systems in monazite. *Chemical Geology*, v. 191, p. 165-181, 2002.
- SPEAR, F. S.; PYLE, J. M.; CHERNIAK, D. Limitations of chemical dating of monazite. *Chemical Geology*, v. 266, p. 227-239, 2009.
- STEIGER, R. H.; JÄGER, E. Subcommission on geochronology: convention on the use of decay constants in geo- and cosmochronology. *Earth and Planetary Science Letters*, v. 36, p. 359-362, 1977.
- SUZUKI, K.; ADACHI, M. Precambrian provenance and Silurian metamorphism of the Tsubonosawa paragneiss in the South Kitakami Terrane, Northeast Japan, revealed by the chemical Th-U-total Pb isochron ages of monazite, zircon and xenotime. *Geochemical Journal*, v. 25, p. 357-376, 1991.
- VLACH, S. R. F. *Geologia e Petrologia dos Granitóides de Morumgaba, SP*. 1993. 414 p. Tese (Doutorado) - Instituto de Geociências, Universidade de São Paulo, São Paulo.
- VLACH, S. R. F.; CAMPOS NETO, M. C.; CABY, R.; BASEI, M. A. S. Contact metamorphism in metapelites from the Nova Lima Group, Rio das Velhas SuperGroup, Quadrilátero Ferrífero: a monazite Th-U-Pb_r dating by the electron-probe microanalyser. In: SOUTH AMERICAN SYMPOSIUM ON ISOTOPE GEOLOGY, 4, 2003, Salvador. *Short Papers...* Salvador, 2003. v. 1, p. 307-310.
- VLACH, S. R. F.; CORREIA, C. T. A comparison between chemical and isotopic dating methods: Th-U-total Pb (monazite, microprobe) and U-Pb (zircon, SHRIMP). In: SOUTH AMERICAN SYMPOSIUM ON ISOTOPE GEOLOGY, 3., 2001, Pucón. *Extended Abstracts ..* Pucón: Sociedad Geologica de Chile, 2001. p. 79-82.
- VLACH, S. R. F.; DANTAS, E. L. Polygenetic monazite from the São José do Campestre Massif, Borborema Province, NE Brazil: insights from EPMA chemical and dating studies. In: SOUTH AMERICAN SYMPOSIUM ON ISOTOPE GEOLOGY, 3., Pucón, 2001. *Extended Abstracts...* Pucón, Sociedad Geologica de Chile, 2001. p. 83-86.
- VLACH, S. R. F.; DEL LAMA, E. A. Idades Th-U-Pb_r de monazita e geotermobarometria de rochas metapelíticas de alto grau do Sistema Orogênico Itabuna-Salvador-Curaçá, BA, Brasil: um estudo em microsonda eletrônica. *Geologia USP. Série Científica*, v. 2, p. 9-22, 2002.
- VLACH, S. R. F.; GUALDA, G. A. R. Microprobe monazite dating and the ages of some granitic and metamorphic rocks from Southeastern Brazil. *Revista Brasileira de Geociências*, v. 30, p. 214-218, 2000.
- VLACH, S. R. F.; GUALDA, G. A. R.; CHIESSI, C. M. Electron microprobe Th-Pb and U-Pb monazite dating. *Acta Microscopica*, v. 8, p. 141-142, 1999a.
- VLACH, S. R. F.; GUALDA, G. A. R.; CHIESSI, C. M. Electron microprobe monazite dating: first results for two granites from Southeastern Brazil. In: SOUTH AMERICAN SYMPOSIUM ON ISOTOPE GEOLOGY, 2, 1999b. Cordoba. *Actas...* Cordoba, 1999b, p. 518-521.
- VLACH, S. R. F.; JANASI, V. A.; ALVES, A. Sistemática de datação de monazita em rochas graníticas: identificação de eventos superpostos no Batólito Natividade da Serra pela combinação de TIMS e EPMA. In: Congresso Brasileiro de Geologia, 41, 2002. João Pessoa. *Anais...* João Pessoa, 2002, p. 511.

WILLIAMS, C. T. Analysis of rare earth minerals. *In*: JONES et al. (Eds.) *Rare Earth Minerals: Chemistry, origin and ore deposits.*, London: Chapman Hall, 1996. p. 327-348. (The Mineralogical Society Series, 7).

WILLIAMS, M. L.; JERCINOVIC, M. J.; TERRY, M. P. Age mapping and dating of monazite on the electron microprobe: Deconvoluting multistage tectonic histories. *Geology*, v. 27, p. 1023-1026, 1999.

WITTKE, J. H. Treatment of analytical data. *Disponível em*: <<http://vishmu.glg.nau.edu/people/jhw/Probe/AnalData.html>>. Acesso em 1998.